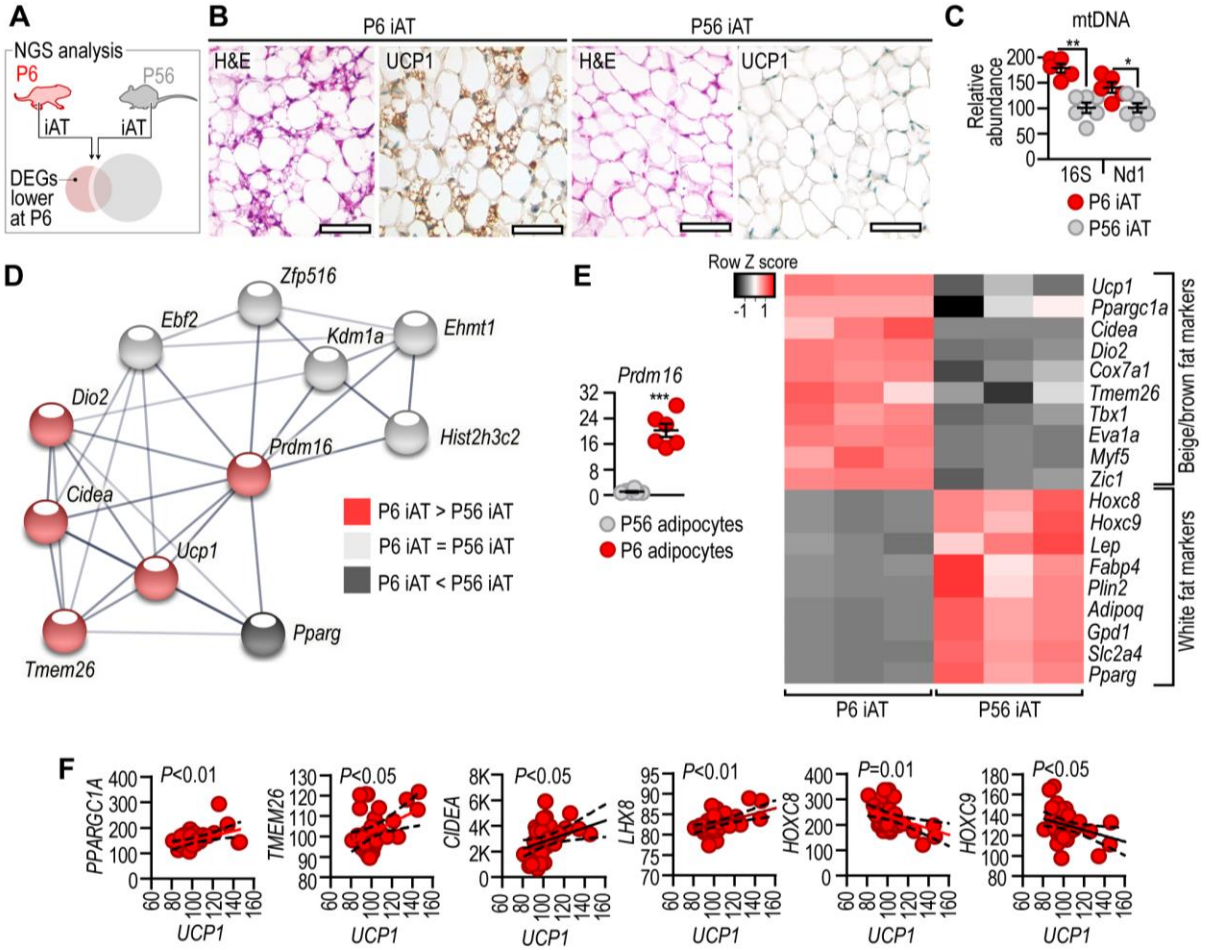

Supplemental Figure 1. Characterization of mouse inguinal adipose tissue at P6 and P56, and human inguinal adipose tissue in infancy

(**A**) Scheme of NGS analysis. For RNA sequencing we obtained inguinal fat depots (iAT) of 3-3 mice at postnatal day 6 (P6) and P56 and compared their transcriptional profiles. The differentially expressed genes (DEGs) were analyzed further in this study. (**B**) Hematoxylin and eosin (H&E) staining, and immunostaining of UCP1 in mouse iAT at P6 and P56. Scale: 50 μm. (**C**) Abundance of mtDNA (*16S* and *Nd1* genes) relative to genomic DNA in mouse iAT at P6 and P56. (**D**) Gene network associated with PR/SET domain 16 (PRDM16), a key regulator of brown adipocyte development (1-3). Red symbols indicate DEGs overrepresented in P6 iAT. Beige/brown adipocyte-associated genes were overrepresented in P6 iAT. (**E**) Transcription of *Prdm16* in mouse adipocytes at P6 and P56. Heat map summarizing the transcription level of beige/brown adipocyte marker genes and white adipocyte marker genes in P6 and P56 iAT. *Ucp1* is necessary for thermogenesis; *Ppargc1a* for mitochondrial biogenesis; *Cidea*, *Cox7a1*, *Dio2*, *Zic1* are associated with brown/beige adipocytes; *Tmem26* and *Tbx1* are beige adipocyte markers; *Eva1a* is a brown adipocyte marker (4-9); *Myf5* is expressed by progenitors of brown adipocytes (10). Levels of *Hoxc8* and *Hoxc9* increase along white adipocyte development (4), although *Hoxc9* may also be a marker of beige adipocytes (9). *Lep*, *Fabp4*, *Plin2*, *Adipoq*, *Gpd1*, *Slc2a4* and *Pparg* are associated with white adipocyte maturation (11). See also (12). (**F**) Correlation of *UCP1* levels with beige/brown adipocyte-associated transcripts (*PPARGC1A*, *TMEM26*, *CIDEA*, *LHX8*) and white adipocyte markers (*HOXC8*, *HOXC9*) in the iAT of human male infants (4, 13). *P* values were determined with linear regression analysis. Age 0.2–3.5 years. Further details regarding beige adipocyte content in mouse and human fat depots are provided in (4, 12-14), and reviewed in the introduction section of (3).

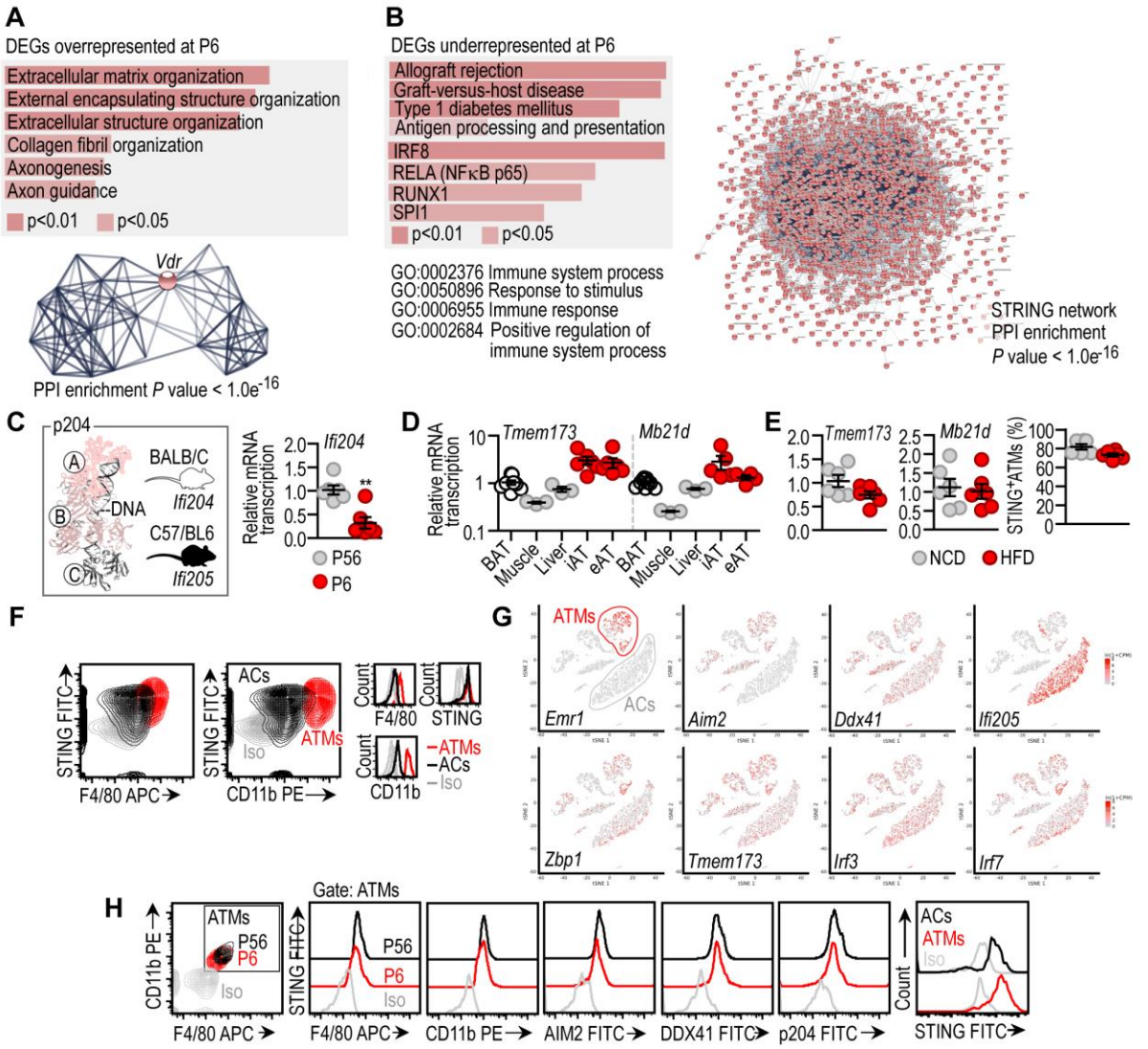

Supplemental Figure 2. Expression of the STING/AIM2 pathways in P6 and P56 iAT
(**A**) Gene ontology and STRING protein-protein association network of DEGs overrepresented in P6 iAT. Further analysis is available in (12). *Vdr* and its gene network were overrepresented at P6. (**B**) Gene ontology and protein-protein association network of underrepresented DEGs at P6 (15). (**C**) Structure of the DNA-sensor p204. The three DNA-binding domains are labeled A, B and C. p204 is encoded by *Ifi204* in BALB/C mice. In C57/BL6, however, *Ifi204* has a frameshift mutation and its function is taken over by *Ifi205* (16-18). In 3T3-L1 cells, which have a BALB/C origin, we measured *Ifi204*, whereas we measured *Ifi205* in adipocytes from C57/BL6 mice. Level of *Ifi204* in P6 and P56-derived adipocytes mirrored that of *Ifi205*, shown in Figure 1. (**D**) Expression of *Tmem173* and *Mb21d* in metabolic organs at P56. Note their prominent expression in iAT and in the epididymal adipose tissue (eAT). (**E**) Level of *Tmem173* and *Mb21d* in iAT of mice fed normal chow diet (NCD) or high-fat diet (HFD). Amount of STING-expressing ATMs in iAT following NCD or HFD. STING expression was not influenced by HFD. (**F**) FACS plot of adipose tissue macrophages (ATMs) and adipocytes (ACs) from iAT. ATMs were defined as F4/80$^+$, CD11b$^+$. (**G**) Single cell sequencing data retrieved from the TabulaMuris consortium (19), showing that the STING pathway is expressed in both ATMs and in adipocytes. There is a marked expression of *Ifi205* in adipocytes. (**H**) FACS analysis of the STING pathway in ATMs at P6 and P56. Gating strategy is provided in (20).

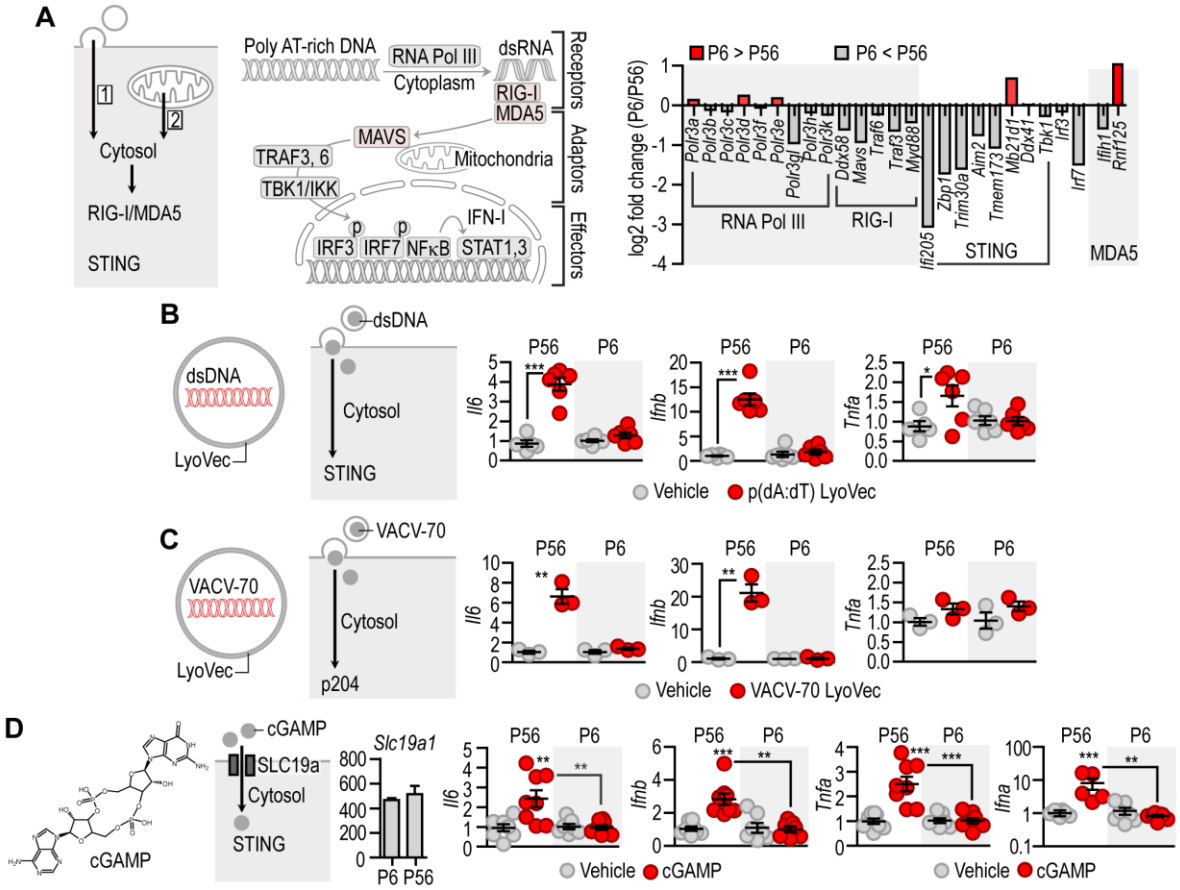

Supplemental Figure 3. Cytosolic DNA sensing in adipocytes

(**A**) *Left:* Possible routes of DNA and RNA release into the cytosol: membrane fusion with EVs [**1**]; release of mtDNA and mtRNA into the cytosol [**2**]. Both mechanisms can activate RIG-I/MDA5 or STING signaling. *Middle:* Scheme of RIG-I/MDA5 signaling. RNA Pol III: RNA polymerase III, which can generate dsRNA from DNA templates, ultimately activating the RIG-I/MDA5 pathway. *Right:* Expression of RNA Pol III and RIG-I/MDA5 pathway genes in P6 iAT. As a comparison, genes of the STING signaling pathway are also shown. See also the heatmap in Figure 1. (**B**) *Left:* Scheme of LyoVec-encapsulated dsDNA. The LyoVec lipid carrier fuses with the cell membrane and dsDNA is released into the cytosol of the recipient cell. *Right:* Responsiveness of P6 and P56 adipocytes to the synthetic dsDNA poly dA:dT (pdA:dT) packed in LyoVec (5 μg/ml, 2 h). (**C**) *Left:* Scheme of LyoVec encapsulated VACV-70 (Vaccinia virus DNA sequence), a ligand for IFI16 in human and p204/p205 in mouse. Responsiveness of P6 and P56 adipocytes to 1 μg/ml VACV-70 (18 h). (**D**) *Left:* Structure of cGAMP and scheme of its entry into the cytosol mediated by the solute carrier SLC19a (21). Transcript level of *Slc19a1* was equivalent in P6 and P56 iAT. *Right:* IFN-response of P6 and P56 iAT after cGAMP treatment (10 μg/ml, 18 h). **P*<0.05, ***P*<0.01, ****P*<0.001. Student's 2-tailed unpaired *t*-test or one-way ANOVA with Dunnett's post-hoc test.

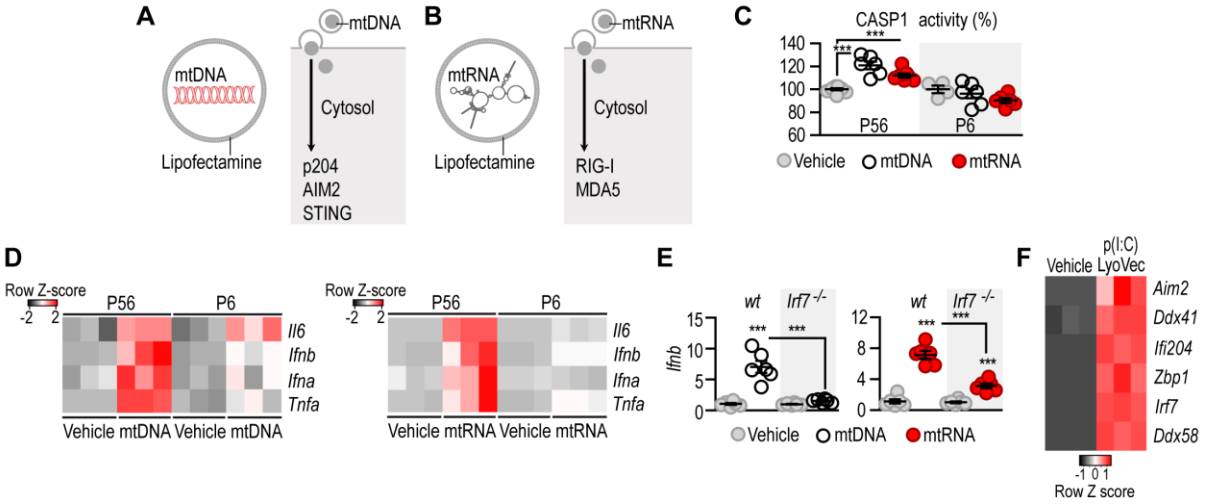

Supplemental Figure 4. Cytosolic mtDNA/mtRNA sensing in adipocytes
(**A**) Scheme of lipofectamine-encapsulated total mtDNA and its delivery into the cytosol of adipocytes. Cytosolic mtDNA is recognized by p204 (IFI16 in humans) and AIM2, and ultimately activates inflammasome and STING signaling. (**B**) Scheme of lipofectamine-encapsulated total mtRNA and its delivery into the cytosol of adipocytes. Cytosolic mtRNA activates RIG-I and MDA5 signaling. (**C**) Inflammasome activation of P56 and P6 adipocytes after 4-h challenge with cytoplasmic mtDNA or mtRNA. CASP1: caspase-1 of the inflammasome (**D**) IFN-response of P56 and P6 adipocytes following transfection with mtDNA or mtRNA (2 µg/ml, 18 h). (**E**) *Ifnb* transcription of wild-type (*wt*) and *Irf7*$^{-/-}$ adipocytes following transfection with vehicle, mtDNA or mtRNA (2 µg/ml, 4 h). (**F**) Transcription of the STING/AIM2 pathway, *Ddx58* and *Irf7* following 18-h activation of IRF7 signaling with LyoVec-encapsulated p(I:C). **P*<0.05, ***P*<0.01, ****P*<0.001. Student's 2-tailed unpaired *t*-test or one-way ANOVA with Dunnett´s post-hoc test.

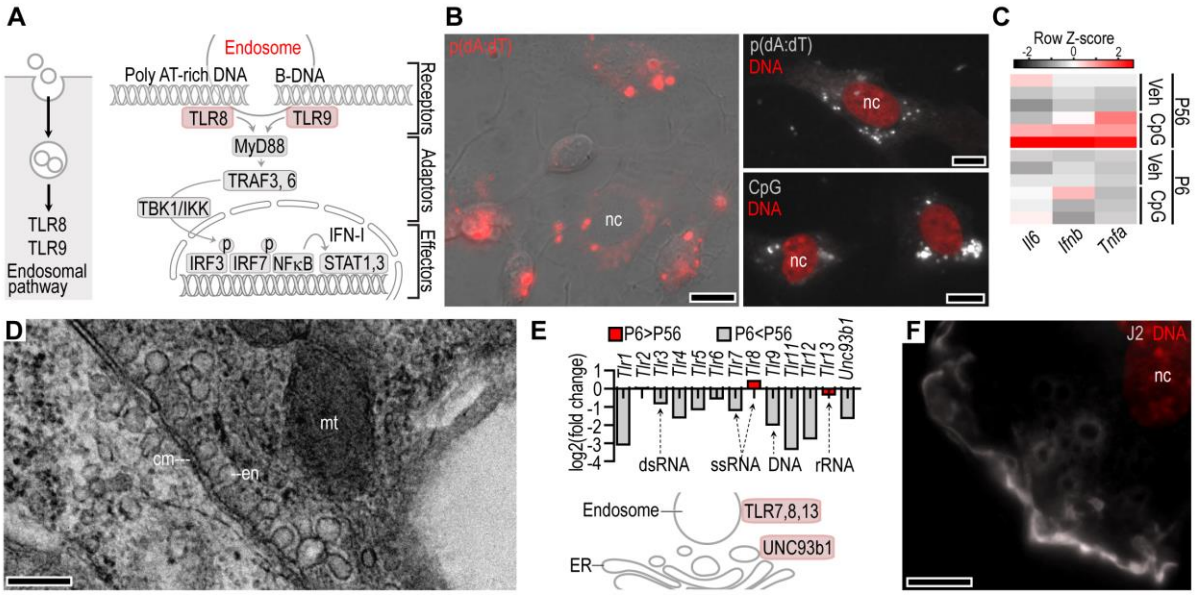

Supplemental Figure 5. Endosomal DNA/RNA sensing in adipocytes

(**A**) Scheme of DNA sensing pathways activated by endosomal uptake of DNA. (**B**) Rhodamine-conjugated naked DNA molecules (p(dA:dT) and CpG) were readily taken up by P6 adipocytes. Scale: 10 μm. (**C**) Effect of naked CpG on inflammatory gene expression in P6 and P56 adipocytes. (**D**) TEM image of two adjacent adipocytes *in vitro*. The cell membranes form numerous endosomes allowing the interchange of EV cargos. en: endosomes; mt: mitochondria; scale: 1 μm. (**E**) Transcript level of TLRs in P6 and P56 iAT. Respective ligands (dsRNA, ssRNA, DNA and rRNA) of the receptors are indicated. Mitochondrial RNA stimulates human TLR8 (22) and triggers inflammation in mouse macrophages mediated by TLR9 (23). (**F**) J2 antibody labeling of dsRNA at the lamellipodia of adipocytes, in an active region of endocytosis (24). nc: nucleus, scale: 10 μm.

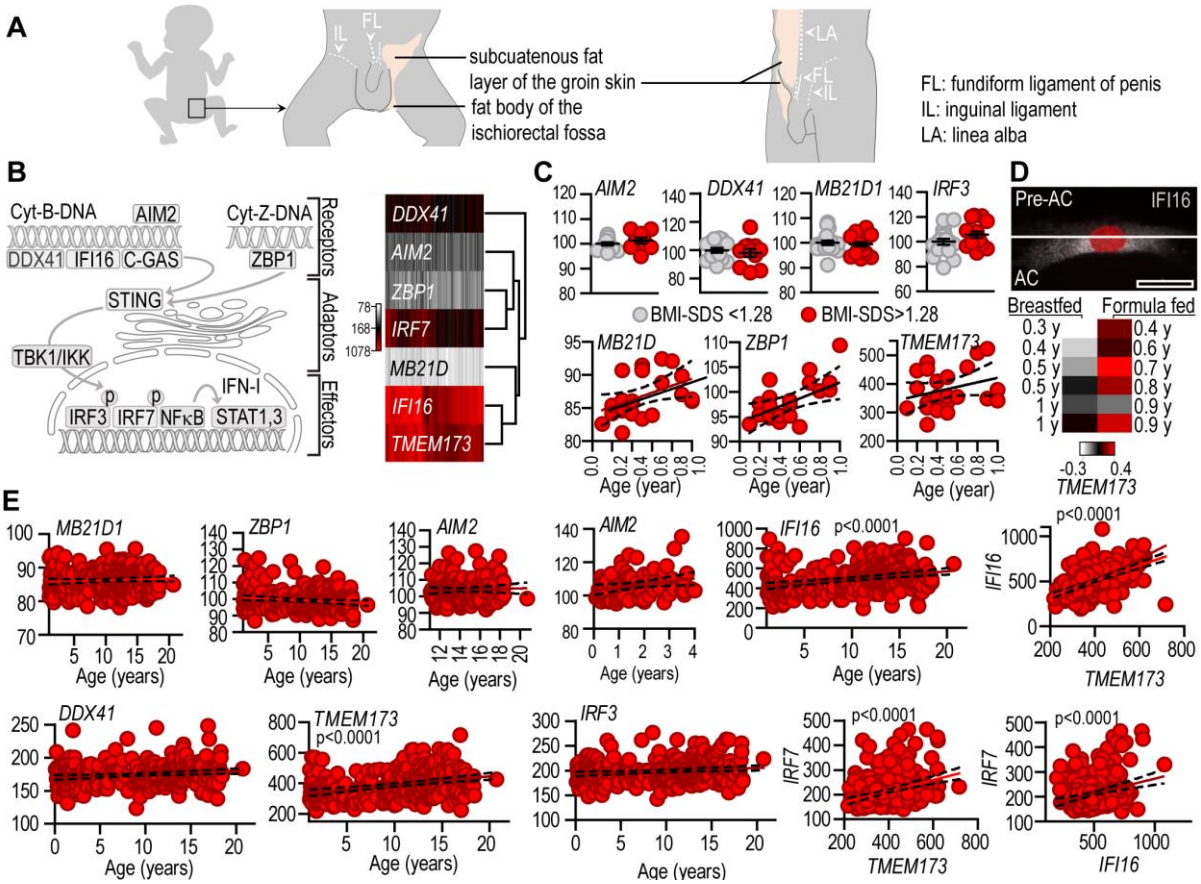

Supplemental Figure 6. STING/AIM2 pathways in human adipose tissue

(**A**) Anatomical sites of human inguinal adipose tissue (iAT) samples used in this study. *Left:* in infants, and *Right*: in children and adults. For proper comparison we used equivalent fat depots in all age groups, from the region bordered by the inguinal ligament, the fundiform ligament of the penis, and the linea alba. (**B**) Scheme of human STING/AIM2 pathways and the relative abundance of their gene products in the iAT collected from human infants (0.2–1.0 years of age, N=24), toddlers (1.1–2.0 years, N=29), children (3.0–11.0 years, N=99), adolescents and young adults (11.1–20.5 years, N=155). (**C**) *Top:* transcript level of adipose tissue *AIM2*, *DDX41*, *MB21D* (encoding cGAS) and *IRF3* in lean (BMI-SDS<1.28) and overweight or obese (BMI-SDS>1.28) infants and children; Illumina HT12v4 assay. *Bottom:* Correlation of age in years (y) and the transcript level of adipose tissue STING/AIM2 pathway genes in human infants. (**D**) *Top:* Immunostaining of IFI16 in a human preadipocyte (Pre-AC) and white adipocyte (AC). Samples from studies (14) and (25). Scale: 50 μm. *Bottom:* Level of adipose tissue *TMEM173* in breastfed and formula-fed infants. Formula-fed infants show premature loss of beige adipocytes in the subcutaneous fat depot (14). (**E**) Transcript level of the human adipose tissue STING/AIM2 pathway genes at various age groups. Correlation between *TMEM173* expression and the level of various DNA sensors. Age group: 0.1–20.5 years. Gender, gestational age, maternal age, maternal diabetes were not correlated with the above parameters. Linear regression analyses with Pearson's correlation.

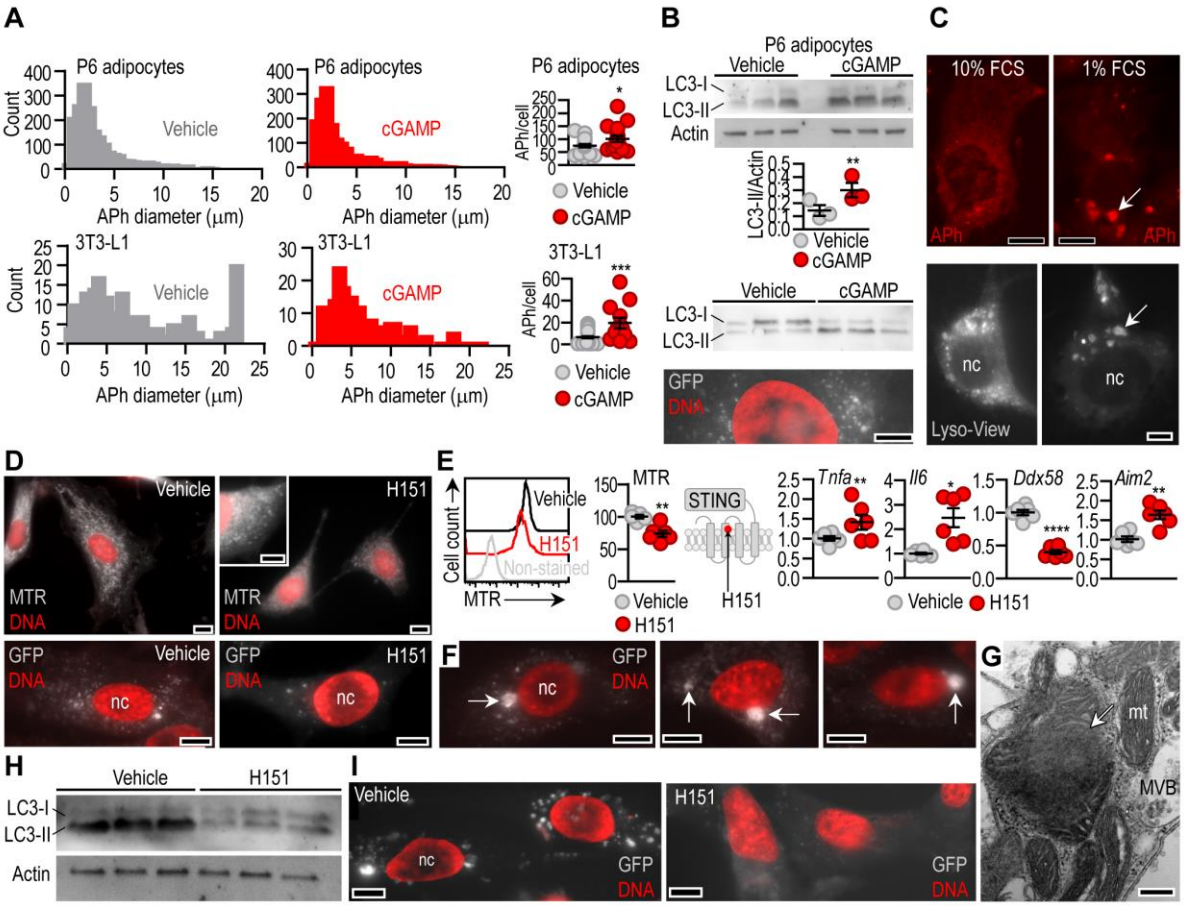

Supplemental Figure 7. STING-mediated mitophagy in P6 adipocytes

(**A**) Autophagosome (APh) number and size in P6 adipocytes and in 3T3-L1 adipocytes treated with vehicle or 5 μg/ml cGAMP for 6h. (**B**) *Top:* Western blotting of LC3 in P6 adipocytes and 3T3-L1 cells treated with vehicle or cGAMP (5 μg/ml, 6 h). *Bottom:* GFP-labeled mitochondrial remnants accumulate in autophagosomes after cGAMP treatment. Scale: 10 μm. (**C**) Autophagosomes and lysosomes (labeled with Lyso-View) in 3T3-L1 cells cultured in 10% fetal calf serum (FCS) or in 1% FCS-containing medium for 18 h. (**D**) Effect of STING inhibition with 0.5 μM H151 on mitochondrial content and morphology in P6 adipocytes. MTR: MitoTracker Red labeling, GFP: GFP labeling of newly synthesized mitochondria with the BacMam 0.2 labeling system, nc: nucleus; scale: 10 μm. (**E**) FACS analysis of MTR labeling of P6 adipocytes, and transcription of inflammatory genes and DNA sensors after 18-h H151 treatment. H151 covalently binds to STING (26). *Ddx58* encodes RIG-I. (**F**) Autophagosomes (arrows) containing GFP-labeled mitochondrial remnants in P6 adipocytes. Scale: 10 μm. (**G**) TEM image of an autophagosome containing mitochondria. mt: mitochondria, MVB: multivesicular body, arrow indicates autophagosome with mitochondrial remnants. Scale: 500 nm. (**H**) Western blotting of LC3 in P6 adipocytes following 6-h serum deprivation. Cells were treated with vehicle or H151 during serum deprivation. (**I**) GFP-labeled mitochondrial remnants in autophagosomes of P6 adipocytes following 6-h serum deprivation. Cells were treated with vehicle or H151 during serum deprivation. Scale: 10 μm. **P*<0.05, ***P*<0.01, ****P*<0.001. Student's 2-tailed unpaired *t*-test.

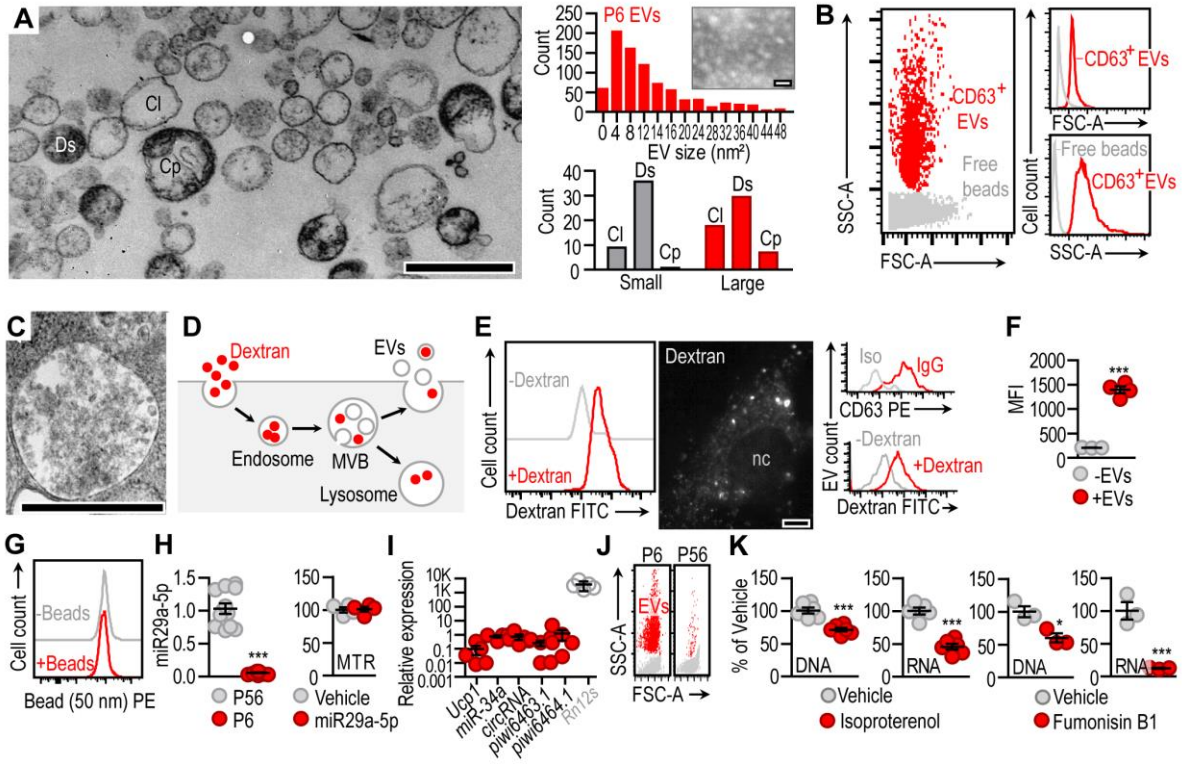

Supplemental Figure 8. Biogenesis of EVs by P6 adipocytes

(**A**) TEM image of EVs released by P6 adipocytes *in vitro.* Scale: 1 μm. Three distinct EV morphologies were recognized: electron-lucent or clear (Cl), electron-dense (Ds) and complex (Cp) EVs. Electron-lucent appearance is typical for EVs (27). Electron-dense EVs may be frequent in EVs within multivesicular bodies (MVBs) (28). Complex EVs contain remnants of intracellular membranes. Size distribution of P6 EVs; *inset* showing negative TEM staining of EVs. Scale: 100 nm. EVs were classified in small and large categories according to a recent study (29). (**B**) FACS analysis of EVs secreted by P6 adipocytes. Free beads: remainder of capture beads used to enrich EVs. (**C**) TEM image of an MVB; scale: 1 μm. (**D**) Endosomal pathway of EV generation was tested by incubating P6 adipocytes with FITC-conjugated dextran, a marker of fluid-phase endocytosis (pinocytosis). Dextran is taken up by endosomes and may later accumulate in MVBs or in lysosomes. (**E**) *Left:* FACS analysis of P6 adipocytes cultured without FITC-conjugated dextran (-Dextran) or after incubation with dextran (+Dextran). *Right:* P6 adipocytes readily endocytosed FITC-dextran, as confirmed with fluorescence microscopy. nc: nucleus; scale: 10 μm. EVs secreted by the dextran-incubated adipocytes were collected and analyzed further with FACS. Dextran was present in the EVs, showing that the endosomal pathway contributed to EV generation. (**F**) Adipocytes were incubated without EVs (-EVs) or with FITC dextran-labeled EVs (+EVs) for 4h. Mean fluorescence intensity (MFI) of the adipocytes was measured by FACS, confirming the uptake of EV cargo by adipocytes. (**G**) Phagocytosis activity of P6 adipocytes was tested with using 50-nm large latex beads. Adipocytes failed to phagocytose these particles, showing that EVs were not taken up by phagocytosis. (**H**) Level of an adipose tissue mesenchymal stem cell-specific microRNA (miR-29a-5p) in P6 and P56 EVs (30). Effect of miR-29a-5p overexpression of the mitochondrial content (MTR fluorescence intensity). (**I**) *Ucp1* and small non-coding RNA species in the EV cargo of P6 adipocytes. As a comparison, the level of the mitochondrially-encoded 12S ribosomal RNA *(Rn12s)* is shown. (**J**) FACS plots of EVs secreted by P6 and P56 adipocytes. (**K**) Inhibitors of EV generation reduced the DNA and RNA content in the culture medium of P6 adipocytes. Isoproterenol (1 μM) inhibits EV release (31), and fumonisin B1 (30 μM) inhibits ceramide synthase, a key enzyme of negative budding of MVBs (32).

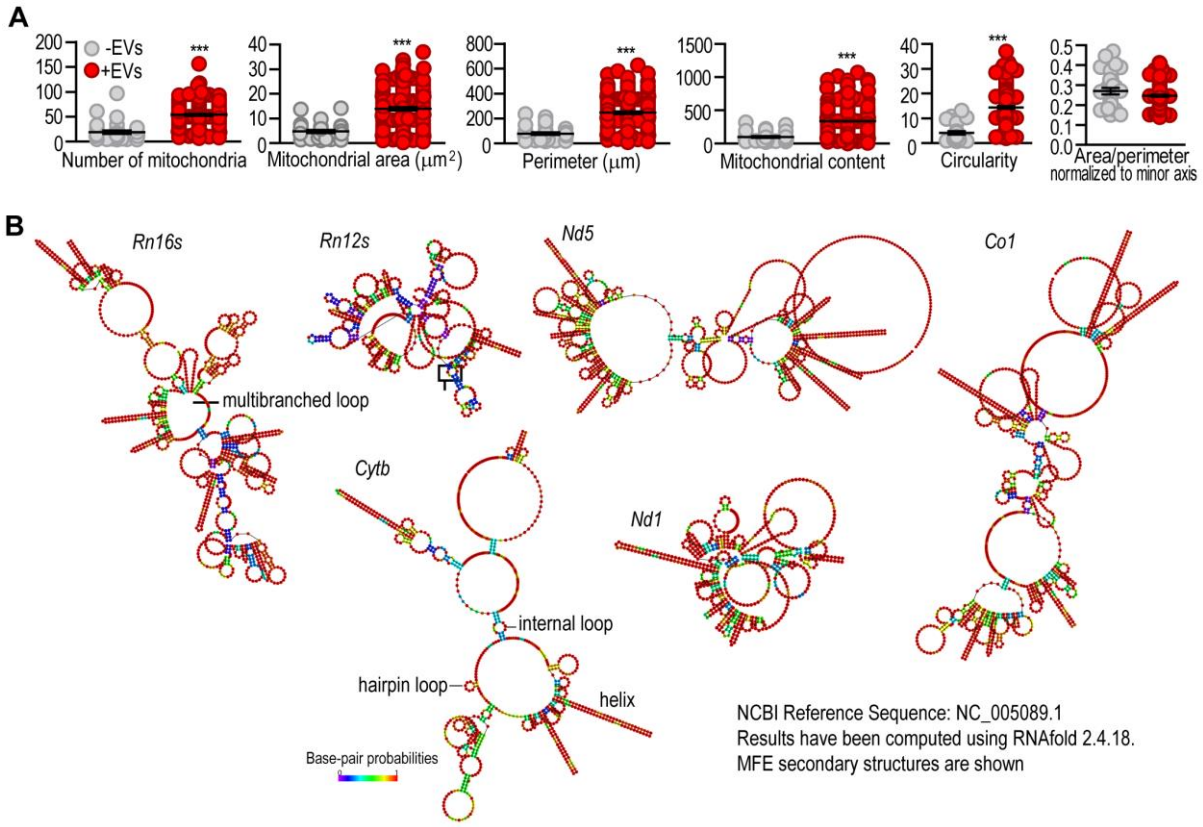

Supplemental Figure 9. Effect of adipocyte EV cargo on mitochondrial morphology, and predicted secondary structure of mtRNA species found in adipocyte EVs
(**A**) Mitochondrial morphometry of 3T3-L1 cells without extracellular vesicles (-EVs) or with P6 EVs (+EVs). ***$P<0.001$. Student's 2-tailed unpaired *t*-test. (**B**) Predicted minimum free energy (MFE) secondary structures of mtRNA species found in P6 EVs. Results were computed using ViennaRNA Package 2.0 and RNAfold 2.2.18, as described (33, 34).

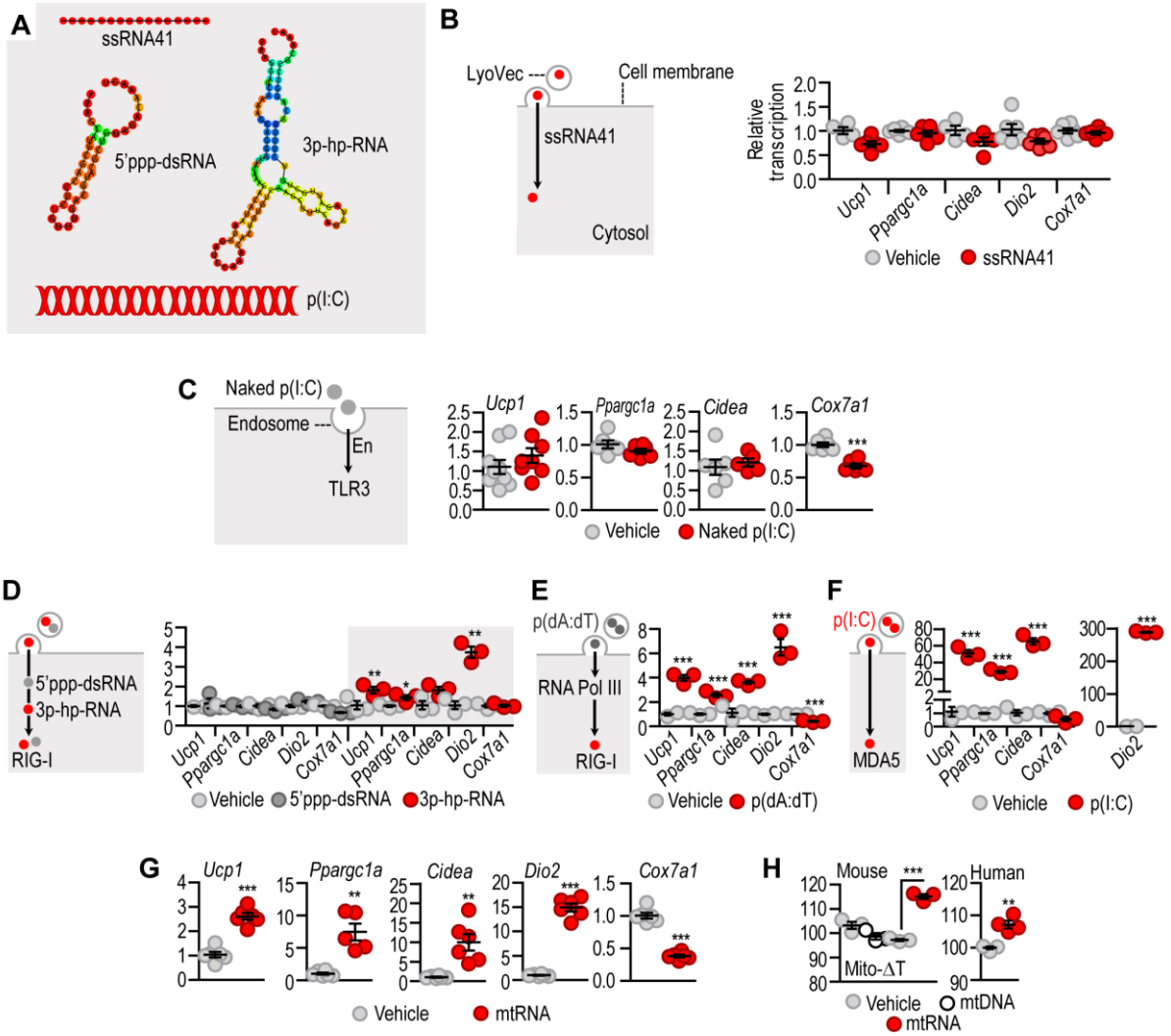

Supplemental Figure 10. Cytosolic and endosomal RNA effects on mitobiogenesis

(A) Secondary and schematic structures of the synthetic ligands used to activate cytosolic RNA sensors. ssRNA41: single-stranded RNA, 3p-hp-RNA: 5' triphosphate hairpin RNA, is an RIG-I ligand (35), 5'ppp-dsRNA: 5' triphosphate dsRNA, a ligand for RIG-I, cytosolic p(I:C) activates MDA5 and RIG-I (36), and cytosolic p(dA:dT) is transcribed into RNA and ultimately activates RIG-I (37). (**B**) Adipocytes were transfected with 2 μg/ml ssRNA41 using the LyoVec transfection system for cytosol delivery. Levels of beige marker genes was measured 18 h after transfection. (**C**) 3T3-L1 cells were treated with 5 μg/ml naked pI:pC to stimulate TLR3 and beige adipocyte gene transcription was then measured 18h after treatment. (**D**,**E**,**F**) Adipocytes were transfected with RIG-I/MDA5 ligands: 5'ppp-dsRNA, 3p-hairpin-RNA, p(dA:dT) and p(I:C) in LyoVec. Levels of beige marker genes was measured 18 h after transfection. (**G**) Transcript level of beige adipocyte genes in P56 adipocytes transfected with mtRNA for 18h. (**H**) Mitochondrial temperature change (Mito-ΔT) measured with the heat-sensitive probe Mitothermo-Yellow (MTY) in mouse and human primary adipocytes. Adipocytes were transfected with vehicle, mtDNA or mtRNA for 18 h. **P*<0.05, ***P*<0.01, ****P*<0.001. Student's 2-tailed unpaired *t*-test.

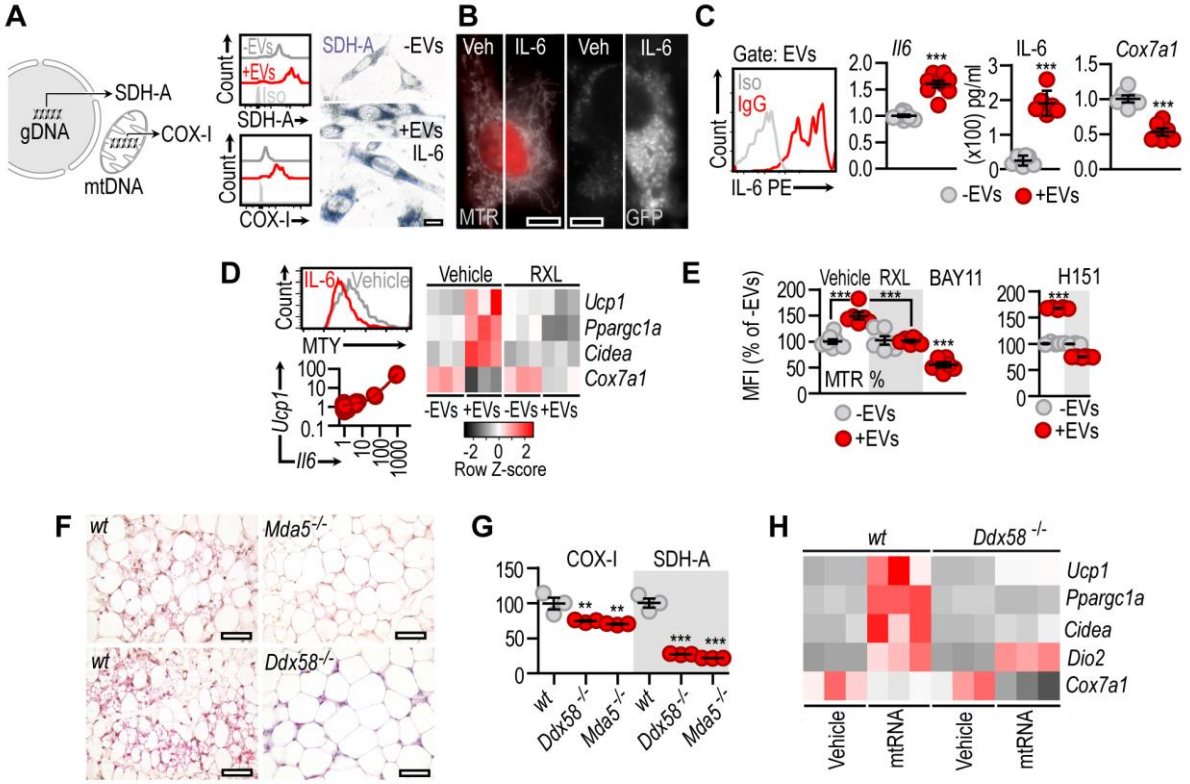

Supplemental Figure 11. IL-6/STAT3 and RIG-I/MDA5 signaling and mitobiogenesis
(**A**) Mitobiogenesis was assessed by measuring SDH-A (succinate dehydrogenase complex, subunit A) and COX-1 (cyclooxygenase 1) by FACS. SDH-A is encoded by genomic DNA (gDNA), COX-I by mtDNA. Representative FACS histograms of COX-I and SDH-A in 3T3-L1 cells after P6 EV treatment. Histochemical staining of SDH-A activity of 3T3-L1 cells cultured without EVs (-EVs), with P6 EVs (+EVs) or with 0.2 ng/ml IL-6 for 18 h. Scale: 10 μm. (**B**) Effect of 200 pg/ml IL-6 on the net mitochondrial mass labeled with MitoTracker Red (MTR), and on the amount of newly synthesized (GFP-expressing) mitochondria. Scale: 50 μm. (**C**) FACS analysis of IL-6 content of P6 EVs. Iso: isotype control; IgG: labeling with anti-IL-6 IgG. Effect of P6 EVs on adipocyte *Il6* expression and IL-6 release. Effect of P6 EVs on *Cox7a1* expression (**D**) Effect of 200 pg/ml IL-6 on the Mitothermo-Yellow (MTY) signal in 3T3-L1 cells. Correlation of *Il6* and *Ucp1* relative expression in adipocytes. Heat map showing expression levels of beige adipocyte genes in 3T3-L1 cells treated with P6 EVs for 18 h. (**E**) MTR signal in 3T3-L1 cells treated with P6 EVs for 18 h. RXL: cells were simultaneously treated with the JAK2/STAT3 inhibitor ruxolitinib; BAY11-7082: cells were treated with an NFκB inhibitor to abrogate the effect of IL-6. (**F**) Histology of iAT from wild-type (*wt*), RIG-I-deficient (*Ddx58*$^{-/-}$) and MDA5-deficient (*Mda5*$^{-/-}$) mice. Note the absence of beige (multilocular) adipocytes in *Ddx58*$^{-/-}$ and *Mda5*$^{-/-}$ mice. Scale 50 μm. (**G**) Mitobiogenesis (relative COX-I and SDH-A levels) in *wt*, *Ddx58*$^{-/-}$ and *Mda5*$^{-/-}$ adipocytes. (**H**) Heat map showing expression levels of beige adipocyte genes in *wt* or *Ddx58*$^{-/-}$ adipocytes treated with vehicle or mtRNA for 18 h. **P*<0.05, ***P*<0.01, ****P*<0.001. Student's 2-tailed unpaired *t*-test.

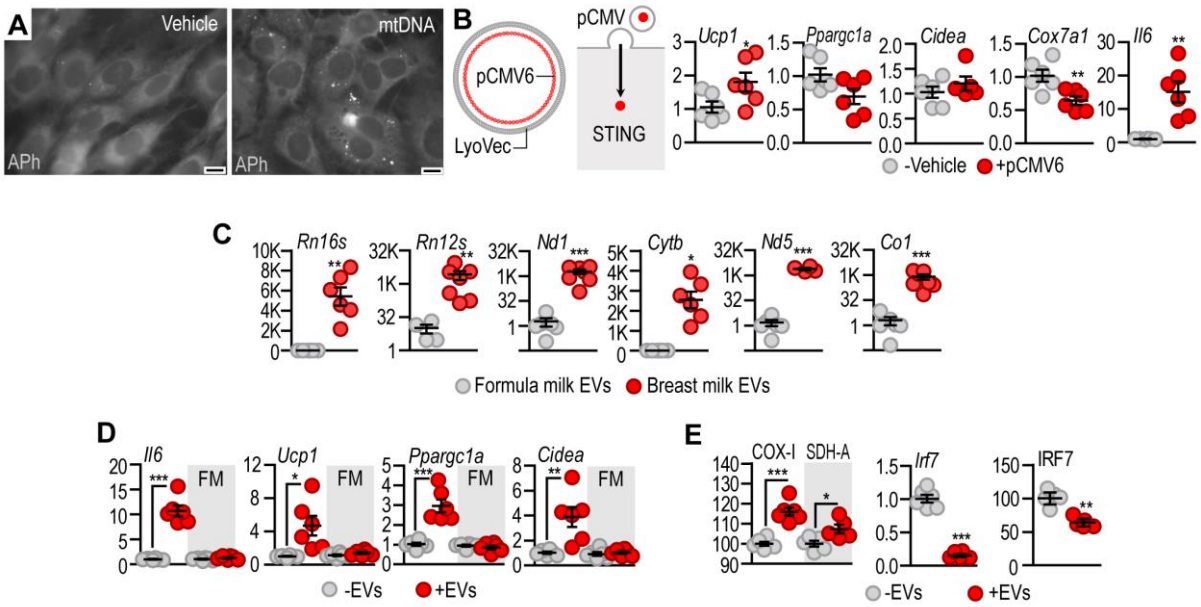

Supplemental Figure 12. Cytosolic DNA/RNA effects on mitobiogenesis
(**A**) Autophagosomes (APh) in P6 adipocytes treated with vehicle or transfected with 2 μg/ml total mtDNA for 18 h. Scale: 10 μm. (**B**) Scheme of LyoVec-encapsulated pCMV6 plasmid – an activator of the c-GAS/STING pathway – and its effect on beige adipocyte gene expression in P6 adipocytes. (**C**) Relative abundance of mtRNA species in human breast milk EVs and commercially available formula milk EVs. (**D**) Effect of breast milk EVs on beige adipocyte gene expression in P56 adipocytes. As a comparison, adipocytes were treated with formula milk-derived EVs (FM). (**E**) Effect of breast milk EVs on the mitobiogenesis of human subcutaneous adipocytes, *Irf7* mRNA levels in mouse adipocytes, and IRF7 protein levels of human adipocytes. Adipocytes were treated with breast milk-derived EVs for 18 h. COX-I: cytochrome oxidase, SDH-A: succinate dehydrogenase, **P*<0.05, ***P*<0.01, ****P*<0.001. Student's 2-tailed unpaired *t*-test.

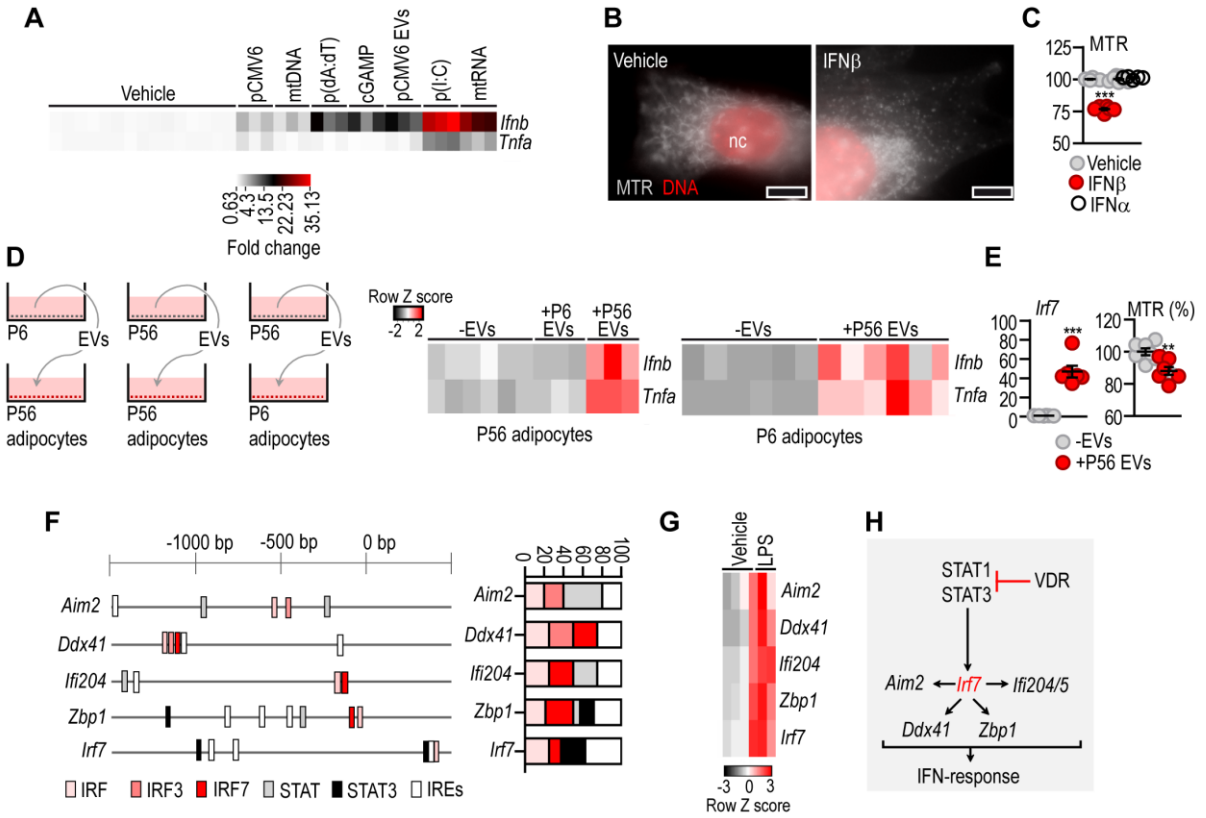

Supplemental Figure 13. IFN-response to EV cargo in adipocytes

(**A**) Effect of cytosolic DNA/RNA on *Ifnb* expression in P56 adipocytes. pCMV6: transfection with pCMV6 plasmid (circular cytosolic DNA), pCMV6 EVs: treatment with extracellular vesicles released by pCMV6 plasmid-transfected adipocytes) (**B**) Effect of IFNβ on the mitochondrial network in P56 adipocytes. Scale: 20 μm. (**C**) Effect of IFNβ and IFNα on mitochondrial mass measured by MitoTracker Red (MTR) staining intensity. Cells were treated with vehicle, 1 pg/ml IFNβ or 1 pg/ml IFNα for 18 h. (**D**) EVs of P6 adipocytes were collected and added to cultures of P56 adipocytes. Similarly, EVs of P56 adipocytes were collected and added to P56 or P6 adipocytes. Levels of *Ifnb* and *Tnfa* were then measured. P6 EVs did not induce IFN-response, whereas P56 EVs triggered a robust IFN-response. (**E**) Transcript level of *Irf7*, and MTR staining intensity in P6 adipocytes treated with P56 EVs. Unlike P6 EVs, which suppressed *Irf7*, P56 EVs stimulated robust *Irf7* expression (see Figure 3C) and reduced mitochondrial content. (**F**) Relative position and percentage of transcription factor binding sites in the promoters of the AIM2/STING pathway and *Irf7*. (**G**) Effect of LPS on the transcription of AIM2/STING pathway and *Irf7* in adipocytes. (**H**) Scheme of the VDR-suppressed signal path which control the expression of *Irf7*, AIM2/STING pathway and IFN-response to cytosolic DNA/RNA (38-41).

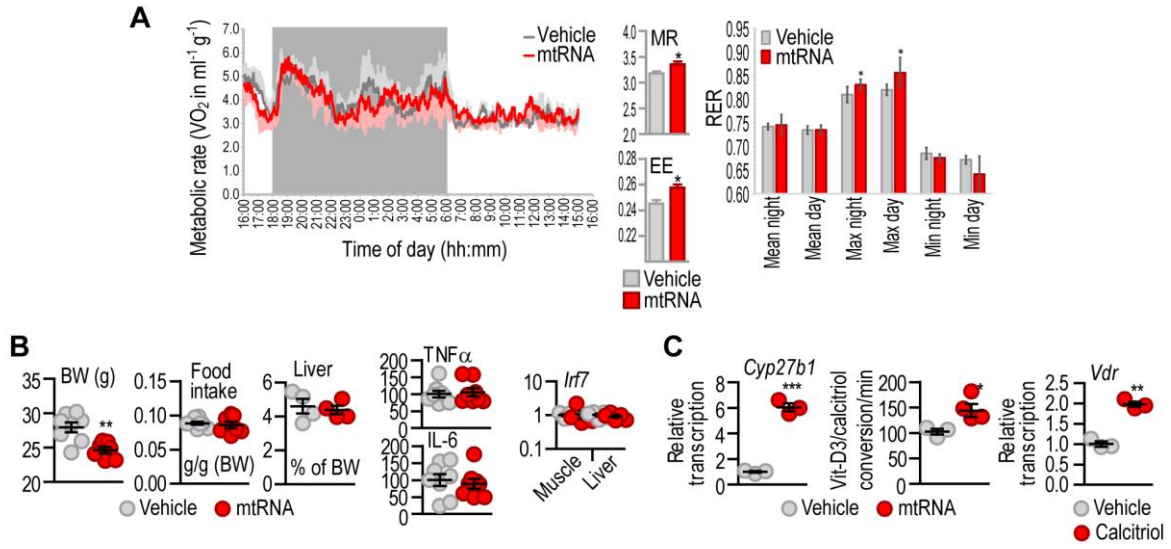

Supplemental Figure 14. Metabolic role of mtRNA-mediated signaling
(**A**) Indirect calorimetry assay of HFD-fed adult male C57BL/6 mice. The inguinal fat depot was transfected with vehicle or with 0.6 μg/g body weight (BW) per day mtRNA for 14 days. The mtRNA was delivered into the adipocyte cytoplasm using magnetofection. Both groups received 4 ng/g BW Vit-D3 daily. MR: metabolic rate, EE: energy expenditure, RER: respiratory exchange rate (**B**) BW, daily food intake normalized to BW, and liver weight normalized to BW. Plasma level of TNFα and IL-6 (% of vehicle) from vehicle- or mtRNA-transfected mice, and the level of *Irf7* in quadriceps muscle and liver. (**C**) *Left:* Transcription of *Cyp27b1* (encoding a Vit-D3/calcitriol converting mitochondrial enzyme) in adipocytes treated with vehicle or transfected with mtRNA for 18h. *Middle:* Rate of Vit-D3/calcitriol conversion in the same cells. *Right:* Effect of calcitriol on the transcription of *Vdr* in adipocytes. **P*<0.05, ***P*<0.01, ***P<0.001. Student's 2-tailed unpaired *t*-test.

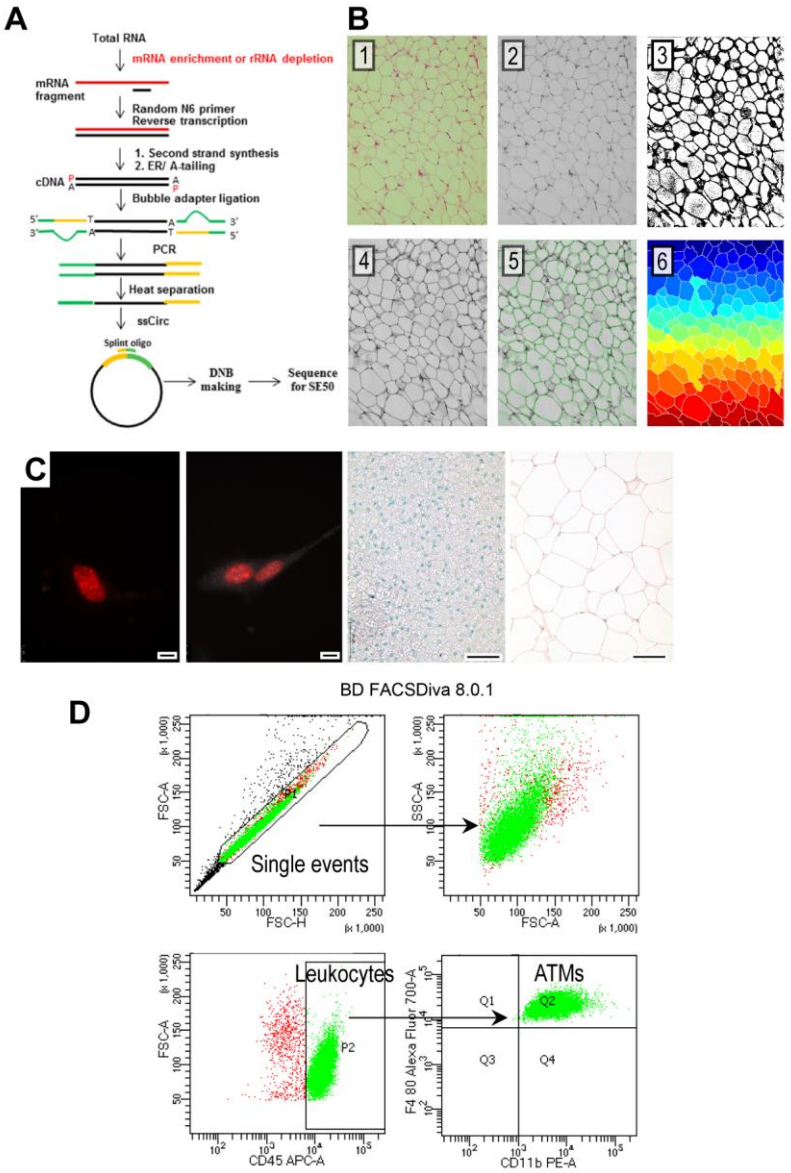

Supplemental Figure 15. Technical information on next-generation sequencing and image analysis

(**A**) Work flow of the next-generation sequencing analysis. (**B**) Steps of image analysis in histomorphometry. (**C**) Negative control specimens. *Left:* Adipocytes *in vitro*, stained with secondary antibodies only; nuclei are labeled with DAPI. Scale: 10 µm. *Middle:* Brown adipose tissue section labeled with secondary antibody only. Scale: 20 µm. Right: human adipose tissue labeled with secondary antibody only. Scale: 20 µm. (**D**) Example of ATM gating strategy. Further details in (20) and (42).

Supplemental Table 1. Mouse qPCR primer sequences used in the study

Bactin	fw	GCACCAGGGTGTGATGGTG
	rev	CCAGATCTTCTCCATGTCGTCC
Ppia	fw	ATTTCTTTTGACTTGCGGGC
	rev	AGACTTGAAGGGGAATG
Gapdh	fw	TGACGTGCCGCCTGGAGAAA
	rev	AGTGTAGCCCAAGATGCCCTTCAG
Aim2	fw	GATTCAAAGTGCAGGTGCGG
	rev	TCTGAGGGTTAGCTTGAGGAC
Ddx41	fw	ACAGGAGAAGCGGTTGCCTTTC
	rev	GACGGCAGTAATACTCCAGGATG
Ifi204	fw	CAGGGAAAATGGAAGTGGTG
	rev	CAGAGAGGTTCTCCCGACTG
Zbp1	fw	AACCCTCAATCAAGTCCTTTACCGC
	rev	TCTTCCACGTCTGTCCGTCATAGCT
Mb21d	fw	AGGAAGCCCTGCTGTAACACTTCT
	rev	AGCCAGCCTTGAATAGGTAGGTAGTCCT
Tmem173	fw	GGGCCCTGTCACTTTTGGTC
	rev	GAGTATGGCATCAGCAGCCAC
Irf3	fw	GGCTTGTGATGGTCAAGGTT
	rev	CATGTCCTCCACCAAGTCCT
Irf7	fw	CGACTTCAGCACTTTCTTCCGAGA
	rev	AGATGGTGTAGTGTGGTGACCCTT
Il6	fw	GCTACCAAACTGGATATAATCAGGA
	rev	CCAGGTAGCTATGGTACTCCAGAA
Tnfa	fw	TGCCTATGTCTCAGCCTCTTC
	rev	GAGGCCATTTGGGAACTTCT
Ifnb	fw	CCAGCTCCAAGAAAGGACGA
	rev	CGCCCTGTAGGTGAGGTTGAT
Ifna	fw	TGAAGGACAGGAAGGACTTTG
	rev	GAATGAGTCTAGGAGGGTTGT
28S	fw	CAGGGGAATCCGACTGTTTA
	rev	ATGACGAGGCATTTGGCTAC
18S	fw	CGCGGTTCTATTTTGTTGGT
	rev	AGTCGGCATCGTTTATGGTC
16S	fw	ACACCGGAATGCCTAAAGGA
	rev	ATACCGCGGCCGTTAAACTT
12S	fw	ACACCTTGCCTAGCCACACC
	rev	GTGGCTGGCACGAAATTTACCA
Nd1	fw	GCTTTACGAGCCGTAGCCCA
	rev	GGGTCAGGCTGGCAGAAGTAA
Cytb	fw	TCCTTCATGTCGGACGAGGC
	rev	AATGCTGTGGCTATGACTGCG
Nd5	fw	GGCCCTACACCAGTTTCAGC
	rev	AGGGCTCCGAGGCAAAGTAT
Co1	fw	TCAACATGAAACCCCCAGCCA
	rev	GCGGCTAGCACTGGTAGTGA

Ucp1	fw	CCTGCCTCTCTCGGAAACAA
	rev	CTGTAGGCTGCCCAATGAAC
Ppargc1	fw	GACTCAGTGTCACCACCGAAA
	rev	TGAACGAGAGCGCATCCTT
Cox7a1	fw	ATGAGGGCCCTACGGGTCTC
	rev	CATTGTCGGCCTGGAAGAG
Cidea	fw	TACTACCCGGTGTCCATTTCT
	rev	ATCACAACTGGCCTGGTTACG
Dio2	fw	GTCCGCAAATGACCCCTTT
	rev	CCCACCCACTCTCTGACTTTC
Ifi205	fw	CAAGCAGGCCACTTCTGTTG
	rev	TCAAACGGGTCTGTTGCAGT
Ddx58	fw	CAAACCGGGCAACAGGAATG
	rev	ATCTCCGCTGGCTCTGAATG
Ifi202b	fw	AAGTTCCCGGCTTGCAGAAC
	rev	TCCAGGAGAGGCTTGAGGTT
Mndal	fw	GACAGCACACTAGAAACCCC
	rev	CTTGTCCTCCATCCAGTCCG
miR34a	fw	TCTTTGGCAGTGTCTTAGCTGG
	rev	ACAATGTGCAGCACTTCTAGGG
circRNA	fw	CTGCTCCTCCAGCTCTT
	rev	AGTGATCTTGAACCCCAAAG
piRNA 6464.1	fw	GGCAAGCTTAGGAGGTGTCC
	rev	CGTGGGTCCACTGTATCACC
piRNA 6463.1	fw	TAAAGCCCTAAAGCCCACGG
	rev	AGGTGTAATGCCAGCCAGTC
Pnpt1	fw	CTTGGACATGGTGCTCTTGC
	rev	GCCAAACTTCCACCACATGC
Adrb3	fw	GTCGTCTTCTGTGTAGCTACGGT
	rev	CATAGCCATCAAACCTGTTGAG
Lipe (Hsl)	fw	AGCCTCATGGACCCTCTTCT
	rev	AGCGAAGTGTCTCTCTGCAC
Atg (Pnpla2)	fw	ACTGAACCAACCCAACCCTT
	rev	CGCACTGGTAGCATGTTGGA
Cyp27b1	fw	AGCTCCTGCGACAAGAAAGT
	rev	ATTCTTCACCATCCGCCGTTA
Vdr	fw	ACTTTGACCGGAATGTGCCT
	rev	CATGCTCCGCCTGAAGAAAC

Supplemental Table 1. (cont.) qPCR primers for measuring mouse mtDNA

Nd1	fw	GCTTTACGAGCCGTAGCCCA
	rev	GGGTCAGGCTGGCAGAAGTAA
16S	fw	ACACCGGAATGCCTAAAGGA
	rev	ATACCGCGGCCGTTAAACTT
12S	fw	ACACCTTGCCTAGCCACACC
	rev	GTGGCTGGCACGAAATTTACCA
D-loop	fw	AATCTACCATCCTCCGTGAAACC
	rev	TCAGTTTAGCTACCCCCAAGTTTAA
Cytb	fw	TCCTTCATGTCGGACGAGGC
	rev	AATGCTGTGGCTATGACTGCG
Atp6	fw	AGCTCACTTGCCCACTTCCT
	rev	AAGCCGGACTGCTAATGCCA
Nd5	fw	GGCCCTACACCAGTTTCAGC
	rev	AGGGCTCCGAGGCAAAGTAT
Co1	fw	TCAACATGAAACCCCCAGCCA
	rev	GCGGCTAGCACTGGTAGTGA
HK2	fw	GCCAGCCTCTCCTGATTTTAGTGT
	rev	GGGAACACAAAAGACCTCTTCTGG

Supplemental Table 1. (cont.) qPCR primers for measuring bovine/human mtRNA

16S	fw	GACTTCACCAGTCAAAGCGA
	rev	ACATCGAGGTCGTAAACCCT
12S	fw	ACTGCTCGCCAGAACACTAC
	rev	GGTGAGGTTGATCGGGGTTT
ND1	fw	GCAGCCGCTATTAAAGGTTCG
	rev	TATCATTTACGGGGGAAGGCG
ND5	fw	TATGTGCTCCGGGTCCATCA
	rev	CTGCTAATGCTAGGCTGCCA
CO1	fw	TCAGGCTACACCCTAGACCA
	rev	CCGGATAGGCCGAGAAAGTG
CYTB	fw	AACTTCGGCTCACTCCTTGG
	rev	CTCGAGTGATGTGGGCGATT

Supplemental Table 1. (cont.) qPCR primers for measuring bovine/human mtDNA

16S	fw	GACTTCACCAGTCAAAGCGA
	rev	ACATCGAGGTCGTAAACCCT
12S	fw	ACTGCTCGCCAGAACACTAC
	rev	GGTGAGGTTGATCGGGGTTT
ND1	fw	GCAGCCGCTATTAAAGGTTCG
	rev	TATCATTTACGGGGGAAGGCG
ND5	fw	TATGTGCTCCGGGTCCATCA
	rev	CTGCTAATGCTAGGCTGCCA
CO1	fw	TCAGGCTACACCCTAGACCA
	rev	CCGGATAGGCCGAGAAAGTG
CYTB	fw	AACTTCGGCTCACTCCTTGG
	rev	CTCGAGTGATGTGGGCGATT

Supplemental Table 2. Antibodies used in the study (h, human; m, mouse)

Target	Cat. No.	IgG type, source
h/m STING	NBP2-24683	Rabbit polyclonal Novus Biologicals, Denver, CO
h/m AIM2	201708-T10	Rabbit polyclonal Sino Biological, Eschborn, Germany
h/m DDX41	102459-T32	Rabbit polyclonal Sino Biological, Eschborn, Germany
h/m p204 (IFI16)	NBP2-27153	Rabbit Polyclonal Novus Biologicals, Denver, CO
h/m ZBP1	207744-T08	Rabbit polyclonal Sino Biological, Eschborn, Germany
h/m LC3	L8918	Rabbit polyclonal, Merck Sigma-Aldrich, St. Louis, MO, Darmstadt, Germany
h/m UCP1	PA1-24894	Rabbit polyclonal ThermoFisher Scientific, Rockford, IL
m NPFF	ab10352	Rabbit polyclonal Abcam, Cambridge, UK
β-actin	NB600-532SS	Rabbit polyclonal Novus Biologicals, Denver, CO
h/m DDX41	102459-T32	Rabbit polyclonal Invitrogen, Carlsbad, CA
h/m Tmem150b	PA5-71527	Rabbit polyclonal Invitrogen, Carlsbad, CA
J2 (dsRNA)	Anti-dsRNA [J2]	Mouse monoclonal Absolute Antibody, Wilton, UK
m IRF7	12-5829-82	PE-conjugated monoclonal IgG, and matching isotype IgG, ThermoFisher, Waltham, MA
m F4/80 antigen m CD11b	sc-377009 E-AB-F1081E	F4/80 APC, IL-6 PE, CD11b APC or PE (FACS analysis), eBioscience, ThermoFisher, Waltham, MA, Santa Cruz Biotech (for IHC)
Rabbit anti-goat IgG	F-2765	H+L, cross-Adsorbed, FITC, polyclonal, secondary antibody, Invitrogen, Carlsbad, CA
Goat anti-rabbit IgG	A16096	Goat anti-Rabbit IgG (H+L), HRP-conjugated Invitrogen, Carlsbad, CA

Supplemental Methods

Activation and inhibition of cytosolic DNA/RNA sensors

To activate STING, we treated adipocytes or 3T3-L1 cells with cGAMP (InvivoGene, Toulouse, France) for 6–18 h, or overexpressed the pCMV6 plasmid (OriGene Technologies, Rockville, MD). In the latter case, 1 μg of DNA was transfected into 300,000 cells using TurboFect Transfection Reagent (Fisher Scientific, Hampton, NH). Control cells received transfection reagent only. Analyses were performed 18-h after transfection. To stimulate RIG-I/MDA5, we transfected 3T3-L1 cells at 80% confluency with high molecular weight polyinosine-polycytidylic acid (p(I:C)) or poly(deoxyadenylic-deoxythymidylic) acid (p(dA:dT)) using the LyoVec cationic lipid-based transfection reagent (InvivoGene, Toulouse, France). Control cells were treated with LyoVec transfection reagent only. We used 2.5–5 μg/ml p(dA:dT) or p(I:C), and cells were analyzed 2–24 h after transfection. IFI16/p204 was activated with 1 μg/ml VACV-70 conjugated to LyoVec transfection reagent (InvivoGene; 18 h) (43). Treatments are summarized in the table below.

Activation of cytosolic nucleic acid sensors with various ligands

Receptor	**Ligand**	**EC_{50}**	**Applied concentration**
STING	2´3 cGAMP	20 nM	10 μg/ml
cGAS	poly(dA:dT) 2h	40-200 ng/ml	2.5-5 μg/ml
	human/mouse mtDNA	-	2 μg/ml
	pCMV6 circular DNA	-	1 μg/well
RIG-I	3p-hpRNA	5 ng/ml	0.5 μg/ml
	5´ppp-dsRNA	1.2 nM	1 μg/ml
	poly(I:C) HMW	70±10 ng/ml	0.5 μg/ml
RIG-I and **MDA5**	poly(dA:dT) 18-24h	40-200 ng/ml	2.5-5 μg/ml
	low molecular weight poly(I:C)	82±8 ng/ml	1 μg/ml
	human/mouse mtRNA	-	2 μg/well
AIM2	poly(dA:dT) 2h	40-200 ng/ml	2.5-5 μg/ml
DDX41	poly(dA:dT) 2h	40-200 ng/ml	2.5-5 μg/ml
	dsDNA (VACV-70)	-	1 μg/ml
IFI16 (p204 or **Ifi204)**	poly(dA:dT) 2h	40-200 ng/ml	2.5-5 μg/ml
	dsDNA (VACV-70)	-	1 μg/ml
ZBP1	poly(dA:dT) 2h	40-200 ng/ml	2.5-5 μg/ml

TLR3 was stimulated with naked p(I:C) (Sigma-Aldrich, 10 ng/ml, 18 h) and TLR8/9 with naked p(dA:dT) or CpG (1 μg/ml synthetic oligonucleotides that contain unmethylated CpG dinucleotides; InvivoGene) for 8 h. STING was inhibited with the irreversible STING inhibitor H-151 (0.5 μM, InvivoGene) (26). As a negative control we used ssRNA (InvivoGene). NFκB was inhibited with 5 μM BAY 11-7082 and JAK2/STAT3 with 280 nM ruxolitinib (Cayman Chemical Company, Ann Arbor, MI). Mitochondrial damage was induced with 10 ng/ml LPS or with CCCP (carbonyl cyanide m-chlorophenyl hydrazone, 1 μM, 15 min treatment).

Vit-D3 and calcitriol were purchased from Sigma-Aldrich; IL-6, IFNα and IFNβ from ImmunoTools (Friesoythe, Germany), NPVF, human and mouse NPFF from Tocris Bioscience (Bristol, UK). Isoproterenol and fumonisin B1 were purchased from Sigma-

Aldrich and from Cayman Chemical Company, respectively. To test the inhibitory effect of Vit-D3 on IRF7 signaling, 3T3-L1 cells were treated with 1 μM Vit-D3 for 48 h, and treated further with vehicle or 5 μg/ml cGAMP for 6 h, or were transfected with mtRNA for 18 h. VDR was inhibited with PS121912, as described (44). Cellular uptake of cGAMP is dependent on the transporter Slc19a1 (21), whose level was similar in P6 and P56 adipocytes (GEO submission #GSE154925).

Isolation of extracellular vesicles from cell culture media, breast milk and formula milk

Extracellular vesicles (EVs) were collected from adipocyte culture media, human breast milk, or from commercially available cattle milk-based infant formula. Human breast milk was collected from healthy volunteers. For cell culture, to avoid contamination with bovine EVs, we used EV-depleted fetal calf serum throughout the study (Gibco). EVs were precipitated with the EPStep exosome precipitation solution (Immunostep, Centro de Investigación del Cáncer, Campus Miguel de Unamuno, Salamanca, Spain) and concentrated by centrifugation. EVs were analyzed with FACS using capture beads and labeling for CD63 (Immunostep). EV pellets were used for treating recipient cells, to extract DNA/RNA, or were processed for FACS. Fractions of EV pellets and adipocytes were also fixed in paraformaldehyde/glutaraldehyde, and processed for transmission electron microscopy (TEM) analysis, as described (42). Morphology of EVs was analyzed with conventional TEM, and with negative staining for TEM (45). EV diameter and area was measured with ImageJ (NIH) with manual annotation, and EVs were classified according to their morphology and electron density, as described (27, 28).

Phagocytosis and endocytosis assays

Uptake of naked nucleic acids was assessed microscopically by incubating adipocytes with rhodamine-conjugated p(dA:dT) or FITC-conjugated ODN 1668 CpG (both from InvivoGene) for 1 h. Endocytosis by means of pinocytosis was assessed by incubating adipocytes with FITC-conjugated dextran, followed by FACS analysis or fluorescence microscopy. Uptake of solid particles was assessed with the use of fluorescent latex beads (Sigma-Aldrich) and FACS analysis (BD LSR II).

ELISA assays

Tissue samples were weighed and homogenized in RIPA buffer using a Roche bead mill homogenizer at 6,500 rpm for 1 min. Cell culture supernatants and plasma samples were centrifuged at 0.8 g for 10 min to remove cell debris, and supernatants were used for analysis. We used commercial ELISA kits to measure the levels of IL-6, TNFα (Fisher Scientific), Vit-D3, calcitriol and VDR (MBS268259-48, MBS2701844-24, MyBioSource). All samples were stored at -80°C until analysis.

mtRNA isolation and *in vitro* transfection

Adipocyte mitochondria were isolated with a commercial mitochondrial isolation kit (Thermo Fisher Scientific, Waltham, MA). Mitochondrial RNA (mtRNA) was isolated by lysing the mitochondrial pellet with TRI Reagent (Sigma-Aldrich), as described (1). 3T3L1 cells were transfected with 2 μg of mtRNA in 6- or 24-well plates with cells at 80–90% confluency. As

a transfection reagent we used Lipofectamine 3000 (Invitrogen) at a 1:3 ratio. Control cells received transfection reagent only. Cells were analyzed 18 h after transfection.

mtDNA isolation and transfection

Mitochondrial DNA (mtDNA)was isolated from mitochondria pellets using TRI Reagent (Merck Sigma-Aldrich) and reconstituted in TE buffer (10 mM Tris-HCL, 1 mM EDTA, pH 8.0). 3T3L1 cells were transfected for 18 h with 1 µg/ml mtDNA using the TurboFect Transfection Reagent. Control cells received transfection reagent only. Agarose gel electrophoresis was used to examine mtDNA integrity.

Cytosolic mtRNA isolation

Cytosol fractions of 3T3-L1 preadipocytes were collected by subcellular fractionation of the cytoplasm and the cell organelles using digitonin, as described (46). Digitonin buffer contained 150 mM NaCl, 50 mM HEPES (pH 7.4) and 25 µg/ml digitonin (D141, Merck Sigma-Aldrich). Treated cells were processed until the step in which cytoplasm was obtained as described (1). 3T3-L1 cytoplasm (250 µl) was added to 750 µl TRI Reagent (T3934, Merck Sigma-Aldrich) and total RNA extraction was performed as described (25).

Histology and image analysis

Tissues were fixed with 4% paraformaldehyde and embedded in paraffin, as described (1). Sections were stained with hematoxylin and eosin (Carl Roth, Karlsruhe, Germany). Antibodies are listed in Supplemental Table 2. UCP1, IFI16, AIM2 and NPFFR1 immunohistochemistry was performed on paraffin-embedded tissue sections. For histomorphometry of fat cells we used Image J, with an image-processing algorithm that incorporated the Euclidean distance-based Watershed transformation to segment the images. Briefly, binarized images were generated using Otsu's method for thresholding; enhanced images were generated using contrast limited adaptive histogram equalization (CLAHE), and finally segmented images were generated using the Watershed transformation (Supplemental Figure 20). Negative control specimens of our fluorescent imaging and immunostaining are shown in Supplemental Figure 15. Mitochondrial content and morphology was analyzed with ImageJ, as described (14). Beige adipose area was measured with our custom-developed image analysis software (BeAR©, (14)).

Oil Red-O staining and quantification of UCP1 staining

The triglyceride content of cultured adipocytes was examined by Oil Red-O using a commercial kit from BioOptica (Milan, Italy), as described (25). *In vitro* UCP1 immunostaining was performed in 6-well culture plates, and samples were imaged and the optical density was measured using digital image analysis. Original images are available upon request through Figshare. Mitochondria were also labeled using an SDH-A histochemistry assay (BioOptica).

Adipocyte differentiation

Mouse preadipocytes of the stromal vascular fraction (SVF) were isolated and maintained as described (25, 42, 47). To ensure the depletion of adipose tissue macrophages (ATMs) from the harvested preadipocytes, we used magnetic bead cell purification of the SVF with an antibody against the F4/80 antigen (Miltenyi Biotec, Bergisch Gladbach, Germany) (20).

Human subcutaneous adipose tissue preadipocytes were harvested as described (25, 42). Preadipocytes were maintained in cell culture medium supplemented with 20 μg/mL insulin. To induce white differentiation of preadipocytes of the SVF, we treated the cells with 50 μM IBMX, 1 μM dexamethasone, 1 μM rosiglitazone and 20 μg/ml insulin (all from Merck Sigma-Aldrich), as described (14).

Flow cytometry analysis of DNA sensors, mitochondrial biogenesis, mitochondrial content and mitochondrial uncoupling

Mitochondrial content was analyzed with MitoTracker dyes (Thermo Fisher Scientific). Mitochondrial biogenesis was detected with the MitoBiogenesis™ Flow Cytometry Kit (Abcam, Cambridge, UK). MitoThermo Yellow (MTY), a temperature-sensitive fluorescent probe (48) was used to assess mitochondrial thermogenesis and uncoupling, as described (49, 50). Temperature difference between the control and the test groups was expressed as Mito-ΔT, and shown in the respective figures. MTY was developed and provided by Dr. Y-T. Chang (Center for Self-Assembly and Complexity, Institute for Basic Science & Department of Chemistry, Pohang University of Science and Technology, Pohang 37673, Republic of Korea). We used MTY for FACS analysis at 0.1 ng/ml to label 10^6/ml cells. Cells were maintained at 37°C throughout the assay. DNA sensors (STING, p204, AIM2, DDX41) were detected with unconjugated antibodies (listed in Supplemental Table 2) and labeled with an FITC-conjugated secondary antibody for FACS analysis. Nucleic acids were labeled with Sytox Green (Thermo Fisher). Flow Repository identifiers of raw FACS data are as follows: #FR-FCM-Z236, #FR-FCM-Z2R6, #FR-FCM-ZYPU, #FR-FCM-ZYUU.

Imaging of mitochondrial content, autophagy and lysosomes

For fluorescent microscopy of mitochondrial content and morphology preadipocytes or 3T3-L1 cells were grown on optical transparent glass-bottom plates (Greiner Bio-One GmbH, Frickenhausen, Germany) or glass coverslips. Functional mitochondria were labeled with MitoTracker Red. Mitochondria were also labeled with GFP using the BacMam 2.0 transfection system (Fisher Scientific). Oxygen consumption was assayed with the Extracellular O_2 Consumption Reagent (Abcam) for 30–120 min. Mitochondrial respiration was evaluated with the WST-81 assay (Carl Roth), as described (51). Autophagosomes and lysosomes were labeled with Cell Meter Autophagy Fluorescence Imaging kit (AAT Bioquest, Sunnyvale, CA), Lyso Brite Orange (Bertin Bioreagent, Montigny le Bretonneux, France) and Lyso View 405 (Biotium, Inc. Fremont, C). Inflammasome activity was measured with the Caspase-Glo 1 Inflammasome Assay (Promega Co., Madison, WI).

High fat diet feeding and indirect calorimetry

Respiratory exchange rate (RER), oxygen consumption (VO_2) and energy expenditure (EE) were measured in each individual mouse for 24 h using a small animal indirect calorimetry system (CaloBox, Phenosys, Germany). Mean RER, VO_2 and EE values were determined over 7 h in the middle of both the day and the night phases. Basal glucose levels and glucose tolerance were measured as described (25). For HFD feeding of mice (dams with litters P6 to P9, or mice at P28 for 12 weeks) we used a rodent HFD from SSNIFF Spezialdiäten (Soest,

Germany) (25). Vit-D3 was supplemented in diet, mtRNA was transfected with magnetofection for 14 days.

miRNA detection

Total RNA was extracted by TRIzol reagent (Invitrogen, Carlsbad, CA, USA) according to the manufacturer's instructions and was quantified using the NanoDrop™ 8000 Fluorospectrometer (Thermo Fisher Scientific). In total, 50 ng of purified RNA was subjected to reverse transcription using a TaqMan miRNA Reverse Transcription Kit and TaqMan® MicroRNA Assays (Applied Biosystems, Foster City, CA) according to the manufacturer's instructions (Assay ID: mmu-miR-434-3p, 002604; mmu-miR-29a-5p, 002447; RUN6B, 001973). Quantification of individual miRNAs was using a QuantStudio™ 12K flex real-time PCR system (Applied Biosystems) and the relative expression values were calculated by using the $2^{-\Delta\Delta Ct}$ method and normalized to *RUN6B*. miR434-3p was overexpressed using a custom-synthesized RNA (Sigma-Aldrich) and transfected with Turbofect transfection reagent (Fisher Scientific). To identify potential *Irf7*-interacting miRNA species, we searched the *TargetScan* database for miRNAs with complementarity to *Irf7* mRNA. In the next step, we used miRBase to identify precursor-, and mature sequences of the candidate miRNA species (52).

Cell viability assay

We used the Presto Blue Cell Viability Assay (Thermo Fisher Scientific) and the Rotitest Vital (Carl Roth) assays according to the manufacturers' instructions.

Western blotting

Cells were lysed in ice-cold RIPA buffer supplemented with Pierce™ protease and phosphatase inhibitor mini tablets (Thermo Scientific). Protein concentration was measured by the Pierce™ Rapid Gold BCA Protein Assay Kit and 30–40 µg protein samples were run on 16% SDS gels for protein separation, followed by blotting the gels on 0.2-µm nitrocellulose blotting membrane (Amersham, Freiberg, Germany) at 300 mA for 1 h in a cold room. After blotting, membranes were blocked with 5% skimmed milk for 1 h. Providers of the β-actin and LC3 antibodies are listed in Supplement Table 2. Antibody concentrations used were as follows: β-actin, 1:10,000, LC3, 0.2 µg/ml.

Quantification of nucleic acids in extracellular vesicles

We collected EV pellets from cells, from formula milk or infant formula in a clean Eppendorf tube, which was centrifuged at 0.8 g to remove cell debris. To isolate the EV-associated DNA from the pellets or from the cell culture media, we used the Zymo Quick DNA Microprep Kit (Zymo Research, Irvine, CA). After determination of the DNA concentration, we used 5 ng for qPCR assays. EV-depleted cell culture media was used as a reference. For comparison between groups, we used the $\Delta\Delta Ct$ method to determine relative changes in mtDNA levels. For extraction of mtRNA and other EV-associated RNA species from cell EV pellets and culture media, we used Trizol Reagent. After determination of the RNA concentration, we used 50 ng of RNA to generate cDNA.

mtDNA copy number in the inguinal adipose tissue

We used Trizol Reagent DNA isolation from iAT at P6 and P56. DNA was reconstituted in TE buffer and adjusted to 10 ng/µl. We performed qPCR using *HK2* as a reference nuclear genome-encoded gene, and measured the DNA copy number of mtDNA-encoded 16S and Nd1. We calculated the copy number according to the formula:

$$\Delta Ct = Ct_{\text{Target gene}} - Ct_{\text{Reference gene}} \quad (1)$$
$$\text{mtDNA copy number} = 2X2^{(\Delta Ct)}$$

Magnetofection of mtRNA

In vivo delivery of mtRNA into the cytosol of adipocytes was achieved with magnetofection, using mtRNA–magnetic nanoparticle complexes (DogtorMag, OzBiosciences, San Diego, CA). Briefly, mtRNA-nanoparticle complexes were injected into the inguinal adipose tissue of mice, and enrichment of the magnetic nanoparticles was ensured by magnetic exposure of the fat depot, as described (53). MicroRNA was transfected using Lipofectamine 3000 (Thermo Fisher).

Institutional Review Board Statement

Research involving animals was approved by the regional governmental ethics and animal welfare committee in Tübingen, Germany (#1511; #1557; #1492; #1546; #o.232-1,2,4,5).

Acknowledgements for the supplemental information

The VDR inhibitor was provided by Prof. Dr. Leggy A. Arnold, University of Wisconsin, USA. MTY was developed and provided by Dr. Y-T. Chang (Center for Self-assembly and Complexity, Institute for Basic Science & Department of Chemistry, Pohang University of Science and Technology, Republic of Korea. The authors thank Prof. Hartmut Geiger (Ulm University) for providing access to the FACS equipment. The assistance of Katharina Schormair and Burak Yildiz in image analysis is much appreciated. The contribution of Vincent Pflüger, Yun Chen, Antonia Stubenvoll, Angelika Bauer are acknowledged. Elements of the 3D artwork used in the graphical abstract was provided by Dreamstime Stock Photography.

References

1. Seale P, Bjork B, Yang W, Kajimura S, Chin S, Kuang S, et al. PRDM16 controls a brown fat/skeletal muscle switch. *Nature.* 2008;454(7207):961-7.
2. Kissig M, Ishibashi J, Harms MJ, Lim H-W, Stine RR, Won K-J, et al. PRDM16 represses the type I interferon response in adipocytes to promote mitochondrial and thermogenic programing. *The EMBO Journal.* 2017;36(11):1528-42.
3. Seale P, Kajimura S, Yang W, Chin S, Rohas LM, Uldry M, et al. Transcriptional control of brown fat determination by PRDM16. *Cell metabolism.* 2007;6(1):38-54.
4. Jespersen NZ, Larsen TJ, Peijs L, Daugaard S, Homøe P, Loft A, et al. A classical brown adipose tissue mRNA signature partly overlaps with brite in the supraclavicular region of adult humans. *Cell Metab.* 2013;17(5):798-805.

5. Kozak LP. The genetics of brown adipocyte induction in white fat depots. *Front Endocrinol (Lausanne).* 2011;2:64.
6. Nascimento EBM, Sparks LM, Divoux A, van Gisbergen MW, Broeders EPM, Jörgensen JA, et al. Genetic Markers of Brown Adipose Tissue Identity and In Vitro Brown Adipose Tissue Activity in Humans. *Obesity.* 2018;26(1):135-40.
7. Perugini J, Bordoni L, Venema W, Acciarini S, Cinti S, Gabbianelli R, et al. Zic1 mRNA is transiently upregulated in subcutaneous fat of acutely cold-exposed mice. 2019;234(3):2031-6.
8. Pilkington A-C, Paz HA, and Wankhade UD. Beige Adipose Tissue Identification and Marker Specificity—Overview. *Front Endocrinol (Lausanne).* 2021;12(8).
9. Carobbio S, Rosen B, and Vidal-Puig A. Adipogenesis: new insights into brown adipose tissue differentiation. *Journal of molecular endocrinology.* 2013;51(3):T75-T85.
10. Sanchez-Gurmaches J, and Guertin DA. Adipocyte lineages: tracing back the origins of fat. *Biochim Biophys Acta.* 2014;1842(3):340-51.
11. Lee K-H, and Kim NH. Differential Expression of Adipocyte-Related Molecules in the Distal Epididymal Fat of Mouse during Postnatal Period. *Development & Reproduction.* 2019;23(3):213-21.
12. Hoang AC, Yu H, and Röszer T. Transcriptional Landscaping Identifies a Beige Adipocyte Depot in the Newborn Mouse. *Cells.* 2021;10(9):2368.
13. Rockstroh D, Landgraf K, Wagner IV, Gesing J, Tauscher R, Lakowa N, et al. Direct evidence of brown adipocytes in different fat depots in children. *PLOS ONE.* 2015;10(2):e0117841.
14. Yu H, Dilbaz S, Coßmann J, Hoang AC, Diedrich V, Herwig A, et al. Breast milk alkylglycerols sustain beige adipocytes through adipose tissue macrophages. *The Journal of Clinical Investigation.* 2019;129(6):2485-99.
15. Szklarczyk D, Gable AL, Lyon D, Junge A, Wyder S, Huerta-Cepas J, et al. STRING v11: protein-protein association networks with increased coverage, supporting functional discovery in genome-wide experimental datasets. *Nucleic acids research.* 2019;47(D1):D607-d13.
16. Luan Y, Lengyel P, and Liu C-J. p204, a p200 family protein, as a multifunctional regulator of cell proliferation and differentiation. *Cytokine Growth Factor Rev.* 2008;19(0):357-69.
17. Bourette RP, and Mouchiroud G. The biological role of interferon-inducible P204 protein in the development of the mononuclear phagocyte system. *Front Biosci.* 2008;13:879-86.
18. Choubey D, and Panchanathan R. Interferon-inducible Ifi200-family genes in systemic lupus erythematosus. *Immunol Lett.* 2008;119(1-2):32-41.
19. Tabula Muris C, Overall c, Logistical c, Organ c, processing, Library p, et al. Single-cell transcriptomics of 20 mouse organs creates a Tabula Muris. *Nature.* 2018;562(7727):367-72.
20. Ampem G, and Röszer T. In: Badr MZ ed. *Nuclear Receptors: Methods and Experimental Protocols*. New York, NY: Springer New York; 2019:225-36.
21. Ritchie C, Cordova AF, Hess GT, Bassik MC, and Li L. SLC19A1 Is an Importer of the Immunotransmitter cGAMP. *Molecular Cell.* 2019;75(2):372-81.e5.
22. Karikó K, Buckstein M, Ni H, and Weissman D. Suppression of RNA Recognition by Toll-like Receptors: The Impact of Nucleoside Modification and the Evolutionary Origin of RNA. *Immunity.* 2005;23(2):165-75.
23. Bakker P, Scantlebery A, Butter L, Claessen N, Teske G, Poll T, et al. TLR9 Mediates Remote Liver Injury following Severe Renal Ischemia Reperfusion. *PloS one.* 2015;10:e0137511.

24. Hines JH, Henle SJ, Carlstrom LP, Abu-Rub M, and Henley JR. Single vesicle imaging indicates distinct modes of rapid membrane retrieval during nerve growth. *BMC Biology.* 2012;10(1):4.
25. Waqas SFH, Hoang A, Lin Y, Ampem G, et al, and Röszer T. Neuropeptide FF increases M2 activation and self-renewal of adipose tissue macrophages. *The Journal of Clinical Investigation* 2017;127(7):2842-54.
26. Haag SM, Gulen MF, Reymond L, Gibelin A, Abrami L, Decout A, et al. Targeting STING with covalent small-molecule inhibitors. *Nature.* 2018;559(7713):269-73.
27. Waldenström A, Gennebäck N, Hellman U, and Ronquist G. Cardiomyocyte Microvesicles Contain DNA/RNA and Convey Biological Messages to Target Cells. *PloS one.* 2012;7:e34653.
28. Zabeo D, Cvjetkovic A, Lässer C, Schorb M, Lötvall J, and Höög JL. Exosomes purified from a single cell type have diverse morphology. *Journal of extracellular vesicles.* 2017;6(1):1329476-.
29. Durcin M, Fleury A, Taillebois E, Hilairet G, Krupova Z, Henry C, et al. Characterisation of adipocyte-derived extracellular vesicle subtypes identifies distinct protein and lipid signatures for large and small extracellular vesicles. *Journal of extracellular vesicles.* 2017;6(1):1305677.
30. Ragni E, Perucca Orfei C, De Luca P, Viganò M, Colombini A, Lugano G, et al. miR-22-5p and miR-29a-5p Are Reliable Reference Genes for Analyzing Extracellular Vesicle-Associated miRNAs in Adipose-Derived Mesenchymal Stem Cells and Are Stable under Inflammatory Priming Mimicking Osteoarthritis Condition. *Stem Cell Reviews and Reports.* 2019;15(5):743-54.
31. Datta A, Kim H, McGee L, Johnson AE, Talwar S, Marugan J, et al. High-throughput screening identified selective inhibitors of exosome biogenesis and secretion: A drug repurposing strategy for advanced cancer. *Scientific Reports.* 2018;8(1):8161.
32. Zitomer NC, Mitchell T, Voss KA, Bondy GS, Pruett ST, Garnier-Amblard EC, et al. Ceramide synthase inhibition by fumonisin B1 causes accumulation of 1-deoxysphinganine: a novel category of bioactive 1-deoxysphingoid bases and 1-deoxydihydroceramides biosynthesized by mammalian cell lines and animals. *The Journal of biological chemistry.* 2009;284(8):4786-95.
33. Narvaez CJ, Matthews D, Broun E, Chan M, and Welsh J. Lean phenotype and resistance to diet-induced obesity in vitamin D receptor knockout mice correlates with induction of uncoupling protein-1 in white adipose tissue. *Endocrinology.* 2009;150(2):651-61.
34. Lorenz R, Bernhart SH, Höner Zu Siederdissen C, Tafer H, Flamm C, Stadler PF, et al. ViennaRNA Package 2.0. *Algorithms for molecular biology : AMB.* 2011;6:26.
35. Hornung V, Ellegast J, Kim S, Brzózka K, Jung A, Kato H, et al. 5'-Triphosphate RNA Is the Ligand for RIG-I. *science.* 2006;314(5801):994-7.
36. Kato H, Takeuchi O, Mikamo-Satoh E, Hirai R, Kawai T, Matsushita K, et al. Length-dependent recognition of double-stranded ribonucleic acids by retinoic acid-inducible gene-I and melanoma differentiation-associated gene 5. *The Journal of experimental medicine.* 2008;205(7):1601-10.
37. Ablasser A, Bauernfeind F, Hartmann G, Latz E, Fitzgerald KA, and Hornung V. RIG-I-dependent sensing of poly(dA:dT) through the induction of an RNA polymerase III–transcribed RNA intermediate. *Nature Immunology.* 2009;10(10):1065-72.
38. Stoppelenburg AJ, von Hegedus JH, Huis in't Veld R, Bont L, and Boes M. Defective control of vitamin D receptor-mediated epithelial STAT1 signalling predisposes to severe respiratory syncytial virus bronchiolitis. *The Journal of Pathology.* 2014;232(1):57-64.

39. Cippitelli M, and Santoni A. Vitamin D3: a transcriptional modulator of the interferon-γ gene. *European Journal of Immunology.* 1998;28(10):3017-30.
40. Helming L, Böse J, Ehrchen J, Schiebe S, Frahm T, Geffers R, et al. 1α,25-dihydroxyvitamin D3 is a potent suppressor of interferon γ–mediated macrophage activation. *Blood.* 2005;106(13):4351-8.
41. Das M, Tomar N, Sreenivas V, Gupta N, and Goswami R. Effect of vitamin D supplementation on cathelicidin, IFN-γ, IL-4 and Th1/Th2 transcription factors in young healthy females. *European Journal of Clinical Nutrition.* 2014;68(3):338-43.
42. Waqas SFH, Noble A, Hoang A, Ampem G, Popp M, Strauß S, et al. Adipose tissue macrophages develop from bone marrow-independent progenitors in *Xenopus laevis* and mouse. *Journal of Leukocyte Biology.* 2017;102(3):845-55.
43. Unterholzner L, Keating SE, Baran M, Horan KA, Jensen SB, Sharma S, et al. IFI16 is an innate immune sensor for intracellular DNA. *Nature immunology.* 2010;11(11):997-1004.
44. Sidhu PS, Teske K, Feleke B, Yuan NY, Guthrie ML, Fernstrum GB, et al. Anticancer activity of VDR-coregulator inhibitor PS121912. *Cancer Chemother Pharmacol.* 2014;74(4):787-98.
45. De Carlo S, and Harris JR. Negative staining and cryo-negative staining of macromolecules and viruses for TEM. *Micron.* 2011;42(2):117-31.
46. Holden P, and Horton WA. Crude subcellular fractionation of cultured mammalian cell lines. *BMC research notes.* 2009;2:243.
47. Hausman DB, Park HJ, and Hausman GJ. Isolation and culture of preadipocytes from rodent white adipose tissue. *Methods in molecular biology.* 2008;456:201-19.
48. Arai S, Suzuki M, Park SJ, Yoo JS, Wang L, Kang NY, et al. Mitochondria-targeted fluorescent thermometer monitors intracellular temperature gradient. *Chemical communications.* 2015;51(38):8044-7.
49. Lane N. Hot mitochondria? *PLoS biology.* 2018;16(1):e2005113.
50. Chrétien D, Bénit P, Ha H-H, Keipert S, El-Khoury R, Chang Y-T, et al. Mitochondria are physiologically maintained at close to 50 °C. *PLoS biology.* 2018;16(1):e2003992.
51. Karabatsiakis A, Böck C, Salinas-Manrique J, Kolassa S, Calzia E, Dietrich DE, et al. Mitochondrial respiration in peripheral blood mononuclear cells correlates with depressive subsymptoms and severity of major depression. *Translational Psychiatry.* 2014;4(6):e397-e.
52. Agarwal V, Bell GW, Nam J-W, and Bartel DP. Predicting effective microRNA target sites in mammalian mRNAs. *eLife.* 2015;4:e05005.
53. Plank C, and Rosenecker J. Magnetofection: The Use of Magnetic Nanoparticles for Nucleic Acid Delivery. *Cold Spring Harbor Protocols.* 2009;2009(6):pdb.prot5230.